2021

CHARACTERIZATION OF IMPACT PILE DRIVING SIGNALS AND FIN WHALE VOCALIZATIONS AT THE BLOCK ISLAND WIND FARM SITE

Jennifer L. Amaral

CHARACTERIZATION OF IMPACT PILE DRIVING SIGNALS AND FIN WHALE VOCALIZATIONS AT THE BLOCK ISLAND WIND FARM SITE

BY

JENNIFER L. AMARAL

A DISSERTATION SUBMITTED IN PARTIAL FULFILLMENT OF THE REQUIREMENTS FOR THE DEGREE OF

DOCTOR OF PHILOSOPHY

IN

OCEAN ENGINEERING

UNIVERSITY OF RHODE ISLAND

2021

DOCTOR OF PHILOSOPHY DISSERTATION

OF

JENNIFER L. AMARAL

APPROVED:

Dissertation Committee:

Major Professor James H. Miller

Gopu R. Potty

Kathleen Vigness-Raposa

Ying-Tsong Lin

Brenton DeBoef

DEAN OF THE GRADUATE SCHOOL

UNIVERSITY OF RHODE ISLAND

2021

ABSTRACT

Offshore wind farm development is rapidly expanding and with that comes the need for assessment of the potential short and long term environmental impacts. As a by-product of the construction, operation, and eventual decommissioning of offshore wind farms, sound is generated both in air and underwater through various activities and mechanisms. With the rate of wind farm development continuing to increase worldwide, regulatory agencies, industry, and scientists are attentive to the potential physiological and behavioral effects these sounds might have on marine life living in the surrounding environment. The impact pile driving used to install the wind turbine foundations is of particular concern due to the intense, impulsive sound that is radiated into the surrounding environment. Piles driven vertically into the seabed generate an azimuthally symmetric underwater sound field whereas piles driven on an angle will generate an azimuthally dependent sound field. Variations in the radiated sound field along opposing azimuths resulted in differences in measured sound exposure levels of up to 10 dB and greater due to the pile rake as the sound propagated in range. This difference in sound levels is significant and should be considered when performing acoustic propagation modeling during the environmental assessment stage of the wind farm development. Environmental assessments are performed to determine how far in range the sound will travel and what potential effect the sound will have on marine animals typically found in the development area. Fin whales are known to traverse the area where the Block Island Wind Farm (BIWF) was constructed and they were recorded vocalizing not long after the foundations for the turbines were installed. Fin whale 20-Hz pulses were recorded for an extended duration and multiple modal arrivals in the received signals were used to localize and track the fin whale. The characteristics of the received signal were then used to invert for the environmental parameters that

supported the observed acoustic propagation.

ACKNOWLEDGMENTS

I wish to thank the members of my committee who have supported me through this entire effort. Jim Miller, Gopu Potty, Ying-Tsong Lin, and Kathy Vigness-Raposa - thank you. I appreciate all of the guidance and encouragement you have provided every step of the way.

I would like to acknowledge my co-authors that have contributed to the success of the manuscripts. Arthur Newhall, Adam Frankel, Daniel Wilkes, and Alexander Gavrilov - thank you for your invaluable input and effort. Also an acknowledgement of the Bureau of Ocean Energy Management (BOEM) who funded the field efforts that collected the data used in my dissertation research. The opportunity to be involved in research on the first offshore wind farm in U.S. waters has been a very rewarding and interesting experience.

Undertaking a doctorate program requires an immense amount of time and effort and I would like to thank my friends and colleagues at Marine Acoustics, Inc. for granting me the flexibility and stability needed to complete this degree. Your continued encouragement and understanding has been very much appreciated.

And of course, I would not be here without the incredible encouragement and support of my friends and family. I can't thank you enough for supporting me through this entire process and cheering me on every step of the way. I could not have achieved this accomplishment without you all on my side. So thank you. I am so grateful.

And Brian - I could not have done this without your endless support. Thank you for always encouraging me and giving me the push I needed to keep at it. This was quite the ride, now on to the next adventure.

PREFACE

The following dissertation is intended in part for the fulfillment of the requirements set forth by the University of Rhode Island Graduate School and the Department of Ocean Engineering for the degree of Doctorate of Philosophy in Ocean Engineering. The purpose of this work is to present an analysis of acoustic data that were collected during the construction of the Block Island Wind Farm, which was the first offshore wind farm in U.S. coastal waters. The Block Island Wind Farm is comprised of five 6-MW turbines located southeast of Block Island, Rhode Island.

The Bureau of Ocean Energy Management (BOEM) funded a project entitled Real-time Opportunity for Development of Environmental Observations (RODEO) to study this wind farm. The goal of this project was to collect real-time measurements of the construction and operation activities from the first offshore wind farm to allow for more accurate assessments of the environmental effects and inform development of appropriate mitigation measures. The University of Rhode Island (URI), Marine Acoustics, Inc. (MAI) and Woods Hole Oceanographic Institution (WHOI) were funded under this project to investigate the acoustics associated with constructing and operating the wind farm. Data analyzed as part of this dissertation were collected through the RODEO program.

This dissertation is presented in manuscript format. The formatting of the manuscripts within this dissertation differ from that in the manuscripts submitted for publication in order to fit the University of Rhode Island formatting guidelines, however, the content is identical to the published manuscripts. The unpublished manuscripts that are part of this dissertation have yet to be submitted to or published in peer-reviewed journals.

Manuscript I was written for Acoustics Today, which is a publication of the

Acoustical Society of America. It is entitled, "The Underwater Sound from Offshore Wind Farms". This article was written as an informational piece for a general scientific audience. The increasing presence of offshore wind farms worldwide was introduced to provide context for the audience before the article presented more detailed information on the different underwater sounds generated during construction, operation, and decommissioning of wind turbines. The types of underwater sounds expected during the life phases of the wind farms were discussed along with ways to mitigate generated sound levels.

Manuscript II was written for publication in the Journal of the Acoustical Society of America as part of a special issue on The Effects of Noise on Aquatic Life. It is entitled, "Characterization of impact pile driving signals during installation of offshore wind turbine foundations". Impact pile driving of multiple steel piles was used to secure the jacket-structure foundations at the Block Island Wind Farm to the seabed. The piles were driven into the sediment on an angle, which resulted in an azimuthally dependent sound field. The underwater acoustic signals from the impact pile driving were recorded at various ranges and analyzed to describe variations in the signal with range and bearing.

Manuscript III has not yet been published or submitted for publication. It is entitled, "Fin whale localization and environmental inversion using modal arrivals of the 20-Hz pulse." Fin whale vocalizations were unintentionally recorded in waters off the coast of Rhode Island during the RODEO program data collection efforts. The vocalizing whale was localized and tracked using multiple modal arrivals of the pulse in the recorded signals. Environmental parameters that supported this type of acoustic propagation were determined through an inversion scheme.

Manuscript IV has not yet been published or submitted for publication. It is entitled, "Analysis and localization of fin whale 20-Hz pulses." This manuscript

presents the fin whale 20-Hz song bout that was recorded. The bout characteristics and localization method are discussed.

TABLE OF CONTENTS

Page

MANUSCRIPT 1

The underwater sound from offshore wind farms

This manuscript was written for Acoustics Today, which is a publication of the Acoustical Society of America. It was featured in the Summer 2020 publication (Volume 16, Issue 2).

Amaral, J., Vigness-Raposa, K., Miller, J. H., Potty, G. R., Newhall, A.,Lin, Y.T. (2020). The Underwater Sound from Offshore Wind Farms. Acoustics Today, 16(2), 13-21. https://doi.org/10.1121/AT.2020.16.2.13.

Jennifer Amaral

Marine Acoustics, Inc, 2 Corporate Place, Suite 105, Middletown, RI 02842, USA

Kathleen Vigness-Raposa

INSPIRE Environmental, 513 Broadway, Newport, RI 02840, USA

James H. Miller and Gopu R. Potty

Department of Ocean Engineering, University of Rhode Island, Narragansett, RI 02882, USA

Arthur Newhall and Ying-Tsong Lin

Applied Ocean Physics and Engineering, Woods Hole Oceanographic Institution, Woods Hole, MA 02543, USA

1.1 Introduction

Efforts to reduce carbon emissions from the burning of fossil fuels have led to an increased interest in renewable energy sources from around the globe. Offshore wind is a viable option to provide energy to coastal communities and has many advantages over onshore wind energy production due to the limited space constraints and greater resource potential found offshore. The first offshore wind farm was installed off the coast of Denmark in 1991, and since then numerous others have been installed worldwide. At the end of 2017, there were 18,814 megawatts (MW) of installed offshore wind capacity worldwide, with nearly 84% of all installations located in European waters and the remaining 16% located offshore of China, followed by Vietnam, Japan, South Korea, the United States, and Taiwan. This equated to 4,149 grid-connected offshore wind turbines in Europe alone, with the number increasing annually since then (Global Wind Energy Council, 2017). In the last 10 years, the average size of European offshore wind farms has increased from 79.6 MW in 2007 to 561 MW in 2018 (Wind Europe, 2018).

On land, China leads the onshore wind energy market with 206 gigawatts (GW) of installed capacity, followed by the United States with 96 GW in 2018 (Global Wind Energy Council, 2019). Over 80% of the US electricity demand is from coastal states, but onshore wind energy generation is usually located far from these coastal areas, which results in long-distance energy transmission. With over 2,000 GW of offshore wind energy potential in US waters, which equals nearly double the electricity demand of the nation, offshore development could provide an alternative to long-distance transmission or development of onshore installations in land-constrained coastal regions (US Department of Energy, 2016). With the potential for offshore wind to be a clean and affordable renewable energy source, US federal and state government interest in development is continuing to grow. The

US Bureau of Ocean Energy Management (BOEM) is responsible for overseeing all the offshore renewable energy development on the outer continental shelf of the United States, which includes issuing leases and providing approval for all potential wind energy projects.

The Block Island Wind Farm (BIWF) was completed in 2016 off the East Coast of the United States in Rhode Island and is the first and only operational wind farm in US waters to date. It produces 30 MW from five 6-MW turbines and is capable of powering about 17,000 homes. As of August 2019, there were 15 additional active offshore wind leases that account for over 21 GW of potential capacity off the East Coast of the United States.

Offshore wind farms are generally constructed in shallow coastal waters, which often have a high biological productivity that attracts diverse marine life. The average water depth of wind farms under construction in 2018 in European waters was 27.1 meters and the average distance to shore was 33 kilometers (Wind Europe, 2018). As a by-product of the construction, operation, and eventual decommissioning of offshore wind farms, sound is generated both in air and underwater through various activities and mechanisms. With the rate of wind farm development continuing to increase worldwide, regulatory agencies, industry, and scientists are attentive to the potential physiological and behavioral effects these sounds might have on marine life living in the surrounding environment. The contribution of sound produced during any anthropogenic activity can change the underwater soundscape and alter the habitats of marine mammals, fishes, and invertebrates by potentially masking communications for species that rely on sound for mating, navigating, and foraging. This article discusses the typical sounds produced during the life of a wind farm, efforts that can be taken to reduce sound levels, and how these sounds might be assessed for their potential environmental impact.

1.2 Construction of Offshore Wind Turbines

Once the development of a wind farm has been approved, the installation of the wind turbine foundations can begin. The type of foundation used will depend on parameters such as the water depth, seabed properties at the site, and turbine size. In water depths less than 50 meters, fixed foundations such as monopiles, gravity base, and jacket foundations are used to secure the wind turbines to the seabed (Figure 1.1). A gravity base foundation is a type of reinforced concrete structure used in water depths less than 10 meters that sits on the seabed and is heavy enough to keep the wind turbine upright. A monopile foundation is a single steel tube with a typical diameter of 3-8 meters that is driven into the seafloor, whereas a jacket foundation is a steel structure composed of many smaller tubular members welded together that sits on top of the seafloor and is secured by multiple steel piles driven into the sediment (Wu et al., 2019). Monopiles can be driven to a depth of 20-45 meters below the seafloor and the piles to secure jacket foundations that can be driven to a depth of between 30 and 75 meters (JASCO and LGL, 2019).

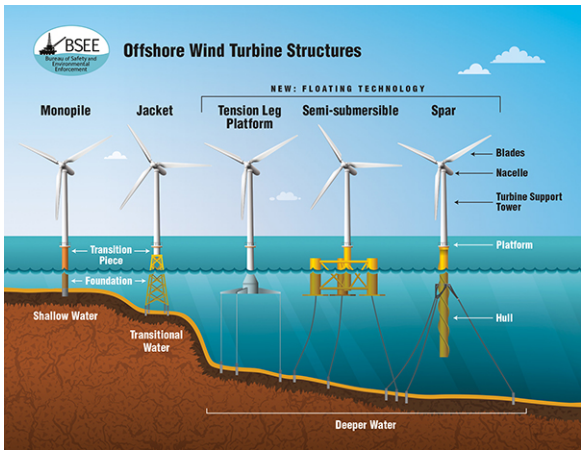

Figure 1.1. Schematic showing some types of offshore wind turbine foundation structures, with the wind turbine components labeled. Image courtesy of the Bureau of Safety and Environmental Enforcement (BSEE), Department of the Interior (see https://tinyurl.com/wawb979).

Most installed wind turbines utilize bottom-fixed foundations, but these foundations become less feasible in water depths greater than 50 meters. In the United States, roughly 58% of the offshore wind potential is in water depths deeper than 60 meters (US Department of Energy, 2016). In these greater water depths, floating foundations that are tethered to the seabed using anchors are a more viable option.

1.3 Impact Pile Driving

Impact pile driving, where the top of the pile is pounded repeatedly by a heavy hammer, is a method used to install monopile and jacket foundations and generates sound in the air, water, and sediment. The installation of a jacket foundation requires multiple piles be driven into the seabed to secure the corners of the steel structure, whereas installation of the monopile design requires one larger pile be driven (Norro et al., 2013). Pile driving is not used for the installation of floating or gravity-based foundations and therefore is not an inherent part of wind farm construction if the water depths and sediment characteristics at the installation

site are suitable for these alternate foundations.

The impact of the hammer on the top of the pile is the primary source of sound that is generated during impact pile driving (see https://tinyurl.com/tbdgsb2). High-amplitude sound pressure is generated that radiates away from the pile on an angle that is dependent on the material properties of the pile and the sound speed in the surrounding water. This angle is typically between 15° and 19° relative to the pile axis (Figure 1.2; Dahl et al., 2015b). Characteristics of the sound generated from each hammer strike are strongly dependent on the pile configuration, hammer impact energy, and environmental properties (such as the water depth and seabed properties).

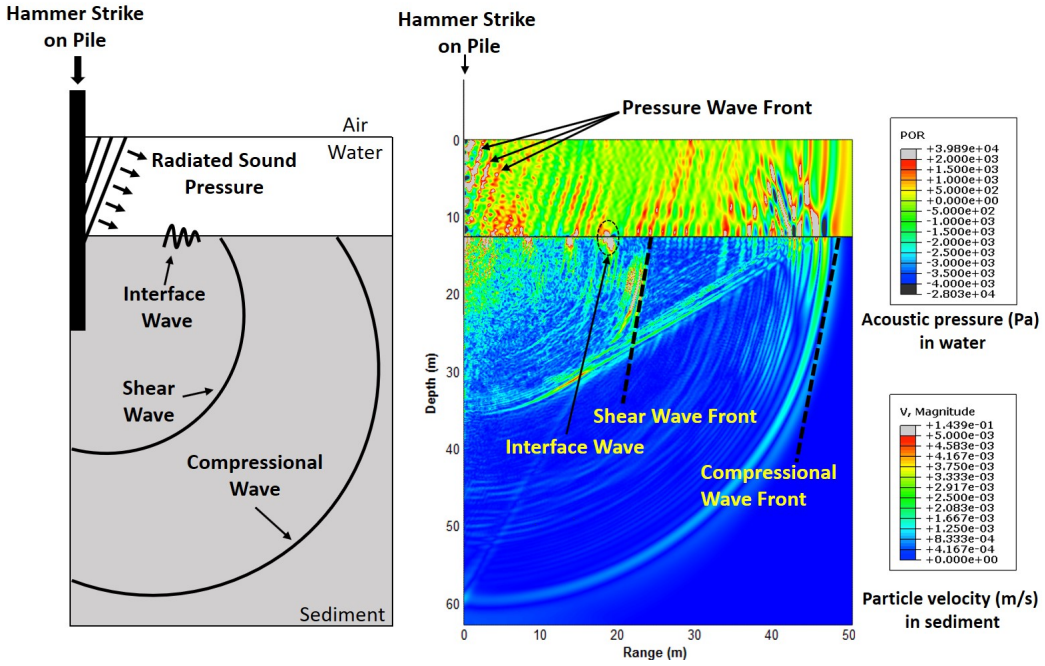

Figure 1.2. Left: simplified schematic showing the types of sound generated as a result of a hammer striking a pile. Sound pressure is radiated into the water at an angle relative to the pile axis, compressional and shear waves are generated in the sediment, and interface waves propagate along the seafloor boundary. Right: finite-element output for the pile driving of a vertical steel pile in 12 meters of water. The seafloor is at 12 meters depth (black horizontal line). The acoustic pressure in the water (<12 meters) and the particle velocity in the sediment (>12 meters) generated from a hammer strike are shown. Various wave phenomena can be seen, including the sound pressure wave radiated at an angle from the pile into the water and the resulting body and interface waves in the sediment. Reprinted/adapted from Popper and Hawkins (2016), with permission from Springer.

In addition to the sound pressure generated in the water, compressional, shear, and interface waves are generated in the seabed that propagate outward from the pile in all directions (Figure 1.2). Compressional waves are the fastest traveling waves in the seafloor and are characterized by particle motion that is parallel to the direction of wave propagation, whereas shear waves, which arrive second, have particle motion that is perpendicular to the direction of the propagating wave (Miller et al., 2016). Interface (or Scholte) waves along the water-sediment interface

occur as a result of interfering compressional and shear waves. The low-frequency and slow-moving interface waves propagate over long distances and generate large-amplitude oscillations along the water-sediment boundary that have the potential to affect marine life living close to or within the seafloor sediment that is sensitive to this type of disturbance (Popper and Hawkins, 2018). The amplitude of the interface wave decays exponentially away from the interface, and, therefore, any disturbance will be noticeable only within a distance of a few wavelengths from the seafloor (Tsouvalas and Metrikine, 2016).

1.3.1 Measuring the Radiated Sound

The total number of hammer strikes required to drive a pile to its final penetration depth could range between 500 to more than 5,000, with the hammer striking the pile between 15 and 60 times per minute (Matuschek and Betke, 2009). On average, a jacket foundation requires three times more hammer strikes to install than a monopile and will result in a longer total piling time because the jacket design requires multiple piles to secure the structure to the seabed as opposed to a single pile for the monopile design (Norro et al., 2013). To characterize the impulsive sound generated during each hammer strike as part of impact pile driving, the sound exposure level (SEL) and peak sound pressure level metrics can be used. The SEL is a measure of the energy within a signal and allows for the total energy of sounds with different durations to be compared. It is defined as the time integral of the squared sound pressure reported in units of decibels re $1\mu\text{Pa}^2\text{s}$. This metric can be used to describe the sound levels from a single strike (SEL_{ss}) and cumulated across multiple hammer strikes or over the duration of the piling activity (SEL_{cum}). When assessing the potential effect of impulsive sounds on the physiology of marine mammals and fishes, the peak sound pressure level and SEL are used (Popper et al., 2014; Southall et al., 2019).

A standard measurement method is important to ensure that independent measurements made at different wind farms can be compared. An approach for measuring and characterizing the underwater sound generated during impact pile driving is defined through the International Organization of Standardization (ISO) 18406 document (2017), which is the standard for measurements of radiated underwater sound from impact pile driving. In this standard, a combination of range-varying hydrophone deployments and fixed-range measurements are recommended to capture variation in the resulting sound field with both distance and changing source characteristics. The source characteristics and resulting sound level radiated into the environment will vary during a piling sequence due to changes in the hammer strike energy, penetration depth of the pile, and depth-dependent seabed properties. Usually, the piling event will begin with hammer strikes at a lower energy before increasing to a higher strike energy to drive the pile deeper into the seafloor. As the length of the pile driven into the seafloor increases, it has the potential to encounter sediment layers with different properties that would influence the resulting radiated sound levels. This variation could be adequately captured on stationary measurement systems, ideally deployed at multiple ranges but with at least one deployed at a range of 750 meters to facilitate comparison with the large number of existing measurements at this range from other wind farm sites (Robinson and Theobald, 2017).

1.3.2 Frequency Content of Hammer Strikes

Impact pile driving radiates considerable levels of low-frequency impulsive noise into the environment. The majority of the energy in the resulting broadband sound field is found below 2 kHz, with spectral peaks between 100 and 400 Hz (Figure 1.3, *top*; Matuschek and Betke, 2009) , where the dispersion of shallow-water acoustic modes is present (Frisk, 1994). Measurements taken during wind

farm construction in the North Sea showed similar spectra resulting from the piling of a monopile and jacket foundation (Norro et al., 2013).

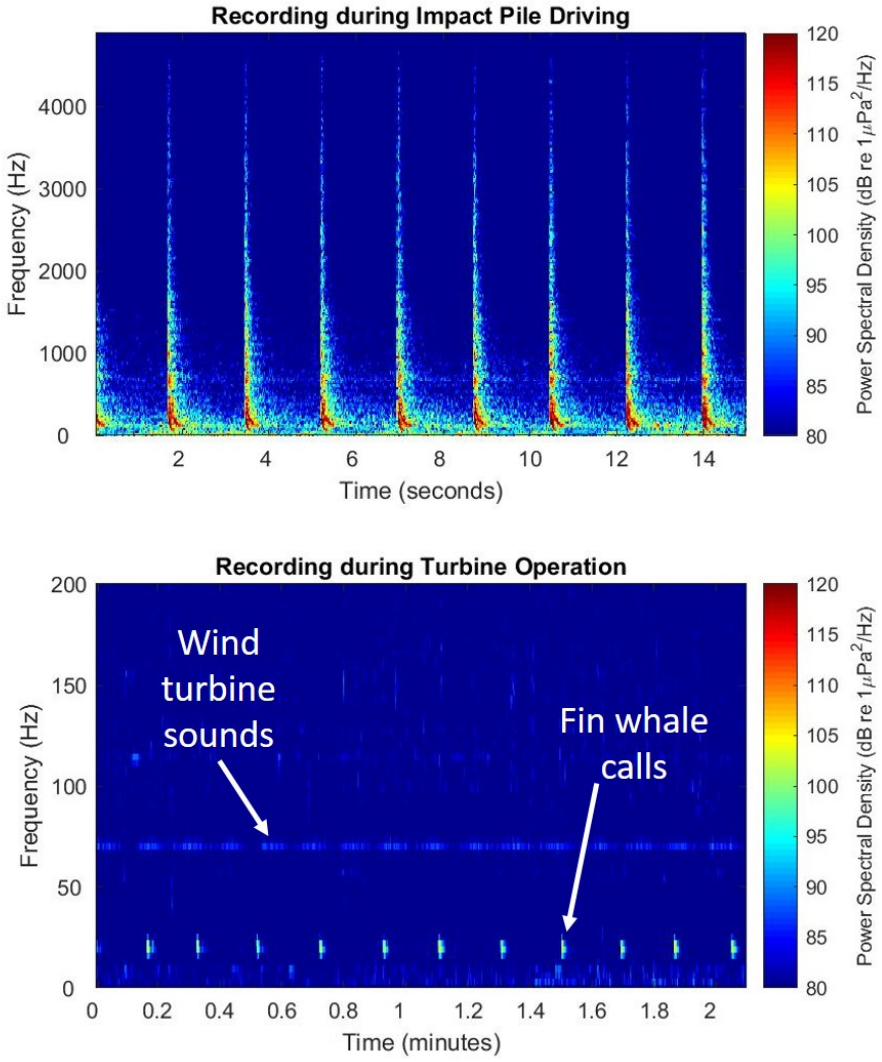

Figure 1.3. Top: time-frequency representation of hammer strikes during impact pile driving at the Block Island Wind Farm (BIWF) recorded at a range of 7.5 kilometers and roughly at midwater depth. Bottom: time-frequency representation of the acoustic signals around 71 Hz hypothesized to be due to the operation of 1 turbine at the BIWF measured near the seafloor at a range of 50 meters while fin whales were vocalizing at 20 Hz. The received wind turbine sounds were measured at a level of 100 dB re 1 μPa root-means-square (rms) while the fin whale vocalizations were measured at a level of 125 dB re 1 μPa rms.

1.3.3 Azimuthal Dependence of Radiated Sound Fields

The installation of jacket foundations sometimes requires piles to be driven on an angle inside the legs of the foundation. For example, the legs of the jacket foundations at the BIWF were hollow, steel members that were inclined inward at an angle of roughly 13° and piles were impact driven into the legs to secure the foundation to the seabed (Figure 4). The nonaxisymmetric orientation of the pile relative to the seabed causes an azimuthal dependence to the radiated sound field, which can result in a significant variation in the received sound levels measured along different radials (Wilkes and Gavrilov, 2017). Received levels recorded on fixed-range and towed measurement systems were substantially different (≈10 dB) between piles inclined in opposite directions (Vigness-Raposa et al., 2017; Martin and Barclay, 2019). These differences were observed independent of the strike energy used for individual hammer strikes (Amaral et al., 2020). The pile orientation affected the incident angle of the radiated pressure wave front on the seabed, which resulted in the directivity of the radiated sound varying based on the azimuth. The steeper the incident angle of the radiated wave front on the seafloor, the more energy was absorbed in the sediment. The azimuthal dependence to the radiated sound field and resulting sound levels are important factors to consider when determining the potential marine mammal and fish impact zones around pile-driving activities for inclined piles.

1.4 Vibratory Pile Driving

Vibratory pile driving is another method used to drive piles into the seafloor and could be used prior to impact pile driving to ensure that the pile is stable in the seabed (JASCO and LGL, 2019) or for the installation of sheet piles to construct temporary cofferdams (Tetra Tech, 2012). In this process, the pile is vibrated at a certain frequency, typically between 20 and 40 Hz, to drive it

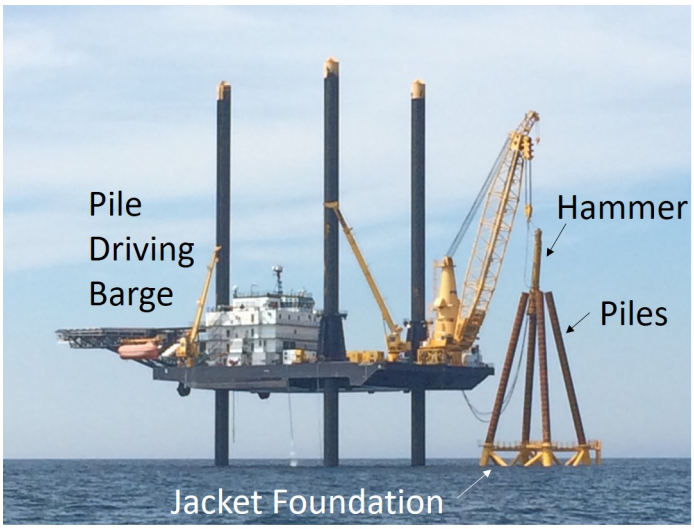

Figure 1.4. Jacket foundation in the water to the right of the pile-driving barge at the BIWF, with a steel pile section inserted into each leg at an angle of roughly 13° prior to piling. The hammer is shown positioned on one of the piles in preparation to drive the pile into the seafloor.

into the sediment rather than hammering the top of the pile (Matuschek and Betke, 2009). The vibratory process produces lower level continuous sounds (see https://tinyurl.com/st4h9tq) compared with the high-amplitude impulsive noise produced during impact pile driving. The high-amplitude pressure waves generated in the water column during impact piling are not present with vibratory piling, and the highest sound pressures are expected near the seafloor as a result of the propagating low-frequency interface waves (Tsouvalas and Metrikine, 2016). The radiated spectrum will be strongly influenced by the vibration frequency, will have peaks at the operating frequency and its subsequent harmonics, and will vary as the operating frequency is adjusted according to changing operational conditions such as sediment type (Dahl et al., 2015a). To assess the impact of nonimpulsive sound on marine life, the SEL metric is used (Southall et al., 2019).

1.5 Additional Construction-Related Sounds

The construction of an offshore wind project generates sound during other activities apart from pile driving, including during the laying of electric cables on the seabed and from the operation of the vessels used during construction. The primary source of noise during the cable laying process is from vessel operations and the potential use of dynamic positioning thrusters to hold vessels in position. An environmental assessment performed for the Vineyard Wind project off the coast of Massachusetts concluded that the sounds generated from these activities were generally consistent with those from routine vessel traffic expected in the area, and, therefore, they were not anticipated to be a significant contributor to the overall acoustic footprint of the project (JASCO and LGL, 2019).

1.6 Operational Sounds of Wind Turbines

The construction of a wind farm takes place over a period of months, whereas the typical wind farm life span is between 20 and 25 years. Once completed, the turbines will operate nearly continuously, except for occasional shutdowns for maintenance or severe weather. Therefore, the contribution of sound to the marine environment will be more consistent and of longer duration during the operational phase than during any other phase of the life of the wind farm (Nedwell and Howell, 2004). The underwater noise levels emitted during the operation of the turbines are low and not expected to cause physiological injury to marine life but could cause behavioral reactions if the animals are in the immediate vicinity of the wind turbine (Tougaard et al., 2009; Sigray and Andersson, 2011).

In some shallow-water environments, sound due to shipping traffic or storms could dominate the low-frequency ambient-sound field over the sound emitted from the wind turbines. Therefore, evaluating the relative sound levels from the wind turbine compared with those from other sources is important when considering

the potential impacts to marine life. Measurements made at three different wind turbines in Denmark and Sweden at ranges between 14 and 40 meters from the turbine foundations found that the sound generated due to turbine operation was only detectable over underwater ambient noise at frequencies below 500 Hz (Tougaard et al., 2009).

The main sources of sound generated during the operation of wind turbines are aerodynamic and mechanical. The mechanical noise is from the nacelle, which is situated at the top of the wind turbine tower and houses the gear box and generator (Figure 1.1). As the wind turbine blades rotate, vibrations are generated that travel down the turbine tower into the foundation and radiate into the surrounding water column and seabed (Tougaard et al., 2009). The resulting sound is described as continuous and nonimpulsive and is characterized by one or more tonal components that are typically at frequencies below 1 kHz (see https://tinyurl.com/wke3lso). The frequency content of the tonal signals is determined by the mechanical properties of the wind turbine and does not change with wind speed (Madsen et al., 2006).

Underwater measurements taken during the operation of one of the turbines at the BIWF contained sound that is hypothesized to be caused by aerodynamic noise from the turbine blade tips that was propagated through the air, into the water, and received on a hydrophone on the seabed at a range of 50 meters (Figure 1.3, *bottom*; J. Miller, Personal observation). This sound was measured to be around 71 Hz and was lower in level than fin whale vocalizations recorded at the same time. This sound was only detectable during times when the weather was calm and there were no ships traveling in the area.

1.7 Sounds from Decommissioning

Since the first offshore wind farm decommissioning in 2015, a small number of offshore farms have been decommissioned, but the decommissioning process is generally unexplored. As more wind farms reach the end of their design life, the decision will have to be made relating to extending operations, repowering, or decommissioning. Decommissioning is typically thought of as a complete removal of all components above and below the water surface, but there is research supporting a partial removal where some of the substructure would remain in place as an artificial reef for marine life (Topham et al., 2019). In general, sound would be generated as a by-product of the process used to remove the substructures, which could include cutting the foundation piles via explosives or water jet cutting (Nedwell and Howell, 2004).

1.8 Assessing Impact to Marine Life

Impulsive sounds, like those generated during impact pile driving, exhibit physical characteristics at the source that make them potentially more injurious to marine life compared with nonimpulsive sounds, like those generated during vibratory pile driving and wind turbine operation (Popper et al., 2014; Southall et al., 2019). Sound exposure is currently assessed based on the sound pressure received in the water column, but the resulting particle motion in the water and sediment is also important when considering the potential impact to marine life sensitive to this stimulus. Additionally, the context under which an animal is exposed to a sound, in addition to the received sound level, will affect the probability of a behavioral response (Ellison et al., 2012).

1.9 Protective Measures to Mitigate Sound Levels

Various mitigation methods can be employed during each phase of wind farm development to reduce the overall propagated sound levels and potential effect on marine life. Time-of-year limitations on construction are implemented to provide safeguards for specific protected or susceptible species. Anti-noise legislation in the Netherlands prohibits pile driving from July 1 through December 31 to avoid disturbance of the breeding season of the harbor porpoise (Tsouvalas and Metrikine, 2016). Off the US East Coast, an agreement was made between environmental groups and a wind farm developer to provide protections for the North Atlantic right whale by not allowing pile driving between January 1 and April 30 when right whales are most likely to be present in the project area (Conservation Law Foundation, 2019).

The use of noise mitigation systems such as bubble curtains (see https://tinyurl.com/v6m6ops) or physical barriers around the pile are commonly used to reduce the levels of sound generated during impact pile driving (Bellmann et al., 2017). These methods are a type of barrier system that work to attenuate the radiated sound levels by exploiting an impedance mismatch between the generated sound wave and a gas-filled barrier. Factors such as the water depth, current, and foundation type will influence the effectiveness of each system.

Ramp-up operational mitigation measures, in which the hammer intensity is gradually increased to full power, are also employed. This method aims to allow time for animals to leave the immediate area and avoid exposure to harmful sound levels, although there are no data to support the contention that this works for fishes, invertebrates, or turtles. Another mitigation method involves visually monitoring an exclusion zone around the piling activity for the presence of marine mammals. This zone is predefined based on the expected sound levels in the area

and requires pausing piling activities if an animal is observed to reduce near-field noise exposure (Bailey et al., 2014).

Exploiting seasonal differences in the water temperature and salinity and its effect on underwater sound propagation could also be used to mitigate the impact of pile-driving noise by scheduling wind farm construction during seasons of high expected acoustic transmission loss. For example, the pile driving for the BIWF occurred during the summer season but had the construction occurred during the winter season, the received SELs at ranges greater than 6 kilometers could have been up to 8 dB higher (Figure 1.5) due to lower water temperatures causing larger acoustic impedance contrast at the seafloor (water-bottom interface) and a more isovelocity, or constant, sound speed profile (Lin et al., 2019). This difference in received sound levels is significant and highlights the effect the environmental conditions have on the overall sound propagation.

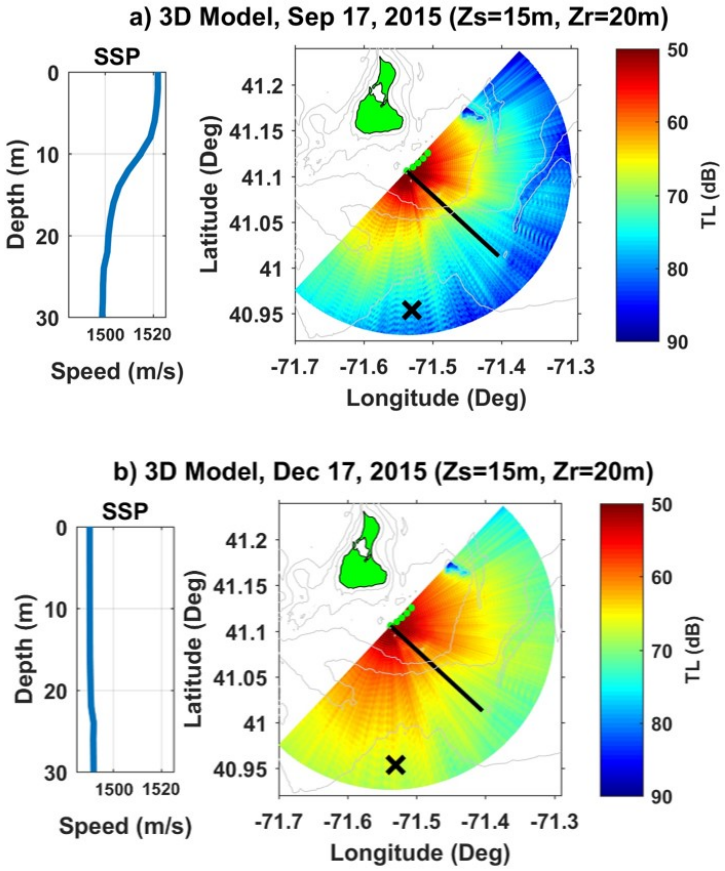

Figure 1.5. Seasonal variability of underwater sound propagation in the BIWF area showing transmission loss (TL) predictions in decibels for a 200 Hz sound source in September 2015 (summer; a) and December 2015 (winter; b). The source depth (Z_s) in the model was 15 meters and the receiver depth (Z_r) was 20 meters. The corresponding sound speed profiles (SSP) are shown. The TL was higher in the summer compared with the winter conditions. Reproduced from Lin et al. (2019), with permission.

1.10 Conclusion

Ancillary sounds of varying levels and characteristics are generated during each phase in the development of an offshore wind farm. The highest amplitude sound is expected during the impact pile-driving part of the construction phase and potentially during the decommissioning phase depending on the methods employed to remove the wind turbine foundations. The installation methods used

for each turbine foundation type will result in different levels and types of sounds radiated into the marine environment. The sound levels can be reduced using physical barriers, and the sound exposure of marine life can be mitigated through monitoring methods and time-of-year restrictions on sound-generating activities. The potential for acute sound exposure of marine mammals and fishes is currently assessed based on the generated sound pressure levels in the water column, but other factors such as the particle motion in the water and sediment and the behavioral response of marine life are important factors to evaluate. Although the construction and decommissioning phases take on the order of months to complete, offshore wind farms are designed to operate for minimum of 20-25 years. With the continued development of offshore wind farms worldwide there will be additional opportunities to measure the underwater sound generated during all phases and assess any potential long-term effect of this sound on the marine environment.

Bibliography

Amaral, J. L., Miller, J. H., Potty, G. R., Vigness-Raposa, K. J., Frankel, A. S., Lin, Y.-T., Newhall, A. E., Wilkes, D. R., and Gavrilov, A. N. (2020). Characterization of impact pile driving signals during installation of offshore wind turbine foundations. *The Journal of the Acoustical Society of America*, 147(4):2323–2333.

Bailey, H., Brookes, K. L., and Thompson, P. M. (2014). Assessing environmental impacts of offshore wind farms: Lessons learned and recommendations for the future. *Aquatic Biosystems*, 10(1):1–13.

Bellmann, M. A., Schuckenbrock, J., Gündert, S., Michael, M., Holst, H., and Remmers, P. (2017). Is There a State-of-the-Art to Reduce Pile-Driving Noise? *Wind Energy and Wildlife Interactions*.

Conservation Law Foundation (2019). Protective Measures for North Atlantic Right Whales.

Dahl, P. H., Dall'Osto, D. R., and Farrell, D. M. (2015a). The underwater sound field from vibratory pile driving. *The Journal of the Acoustical Society of America*, 137(6):3544–3554.

Dahl, P. H., de Jong, C. A., and Popper, A. N. (2015b). The Underwater Sound Field from Impact Pile Driving and Its Potential Effects on Marine Life. *Acoustics Today*, 11(2):18–25.

Ellison, W. T., Southall, B. L., Clark, C. W., and Frankel, A. S. (2012). A New Context-Based Approach to Assess Marine Mammal Behavioral Responses to Anthropogenic Sounds. *Conservation Biology*, 26(1):21–28.

Frisk, G. V. (1994). *Ocean and Seabed Acoustics*. Prentice-Hall, Inc, Englewood Cliffs, New Jersey.

Global Wind Energy Council (2017). GWEC Global Wind 2017 Report - A snapshot of top wind markets in 2017: Offshore wind. Technical report, Global Wind Energy Council.

Global Wind Energy Council (2019). Global Wind Report 2018. Technical Report April, Global Wind Energy Council, Brussels, Belgium.

ISO (2017). *ISO 18406 Underwater acoustics - Measurement of radiated underwater sound from percussive pile driving*. International Organization for Standardization, Geneva, Switzerland.

JASCO and LGL (2019). Request for an Incidental Harassment Authorization to Allow the Nonlethal Take of Marine Mammals Incidental to Construction Activities in the Vineyard Wind BOEM Lease Area OCS. Technical report, Prepared by JASCO Applied Sciences (USA) Ltd. and LGL Ecological Research Associates, for Vineyard Wind, LLC, Version 4.1, Document No. 01648.

Lin, Y.-T., Newhall, A. E., Miller, J. H., Potty, G. R., and Vigness-Raposa, K. J. (2019). A three-dimensional underwater sound propagation model for offshore wind farm noise prediction. *The Journal of the Acoustical Society of America*, 145(5):EL335–EL340.

Madsen, P. T., Wahlberg, M., Tougaard, J., Lucke, K., and Tyack, P. (2006). Wind turbine underwater noise and marine mammals: Implications of current knowledge and data needs. *Marine Ecology Progress Series*, 309(Tyack 1998):279–295.

Martin, S. B. and Barclay, D. R. (2019). Determining the dependence of marine pile driving sound levels on strike energy , pile penetration , and propagation

effects using a linear mixed model based on damped cylindrical spreading. *The Journal of the Acoustical Society of America*, 146(1):109–121.

Matuschek, R. and Betke, K. (2009). Measurements of Construction Noise During Pile Driving of Offshore Research Platforms and Wind Farms. *NAG/DAGA International Conference on Acoustics*, pages 262–265.

Miller, J. H., Potty, G. R., and Kim, H.-K. (2016). Pile-Driving Pressure and Particle Velocity at the Seabed: Quantifying Effects on Crustaceans and Groundfish. In Popper, A. N. and Hawkins, A. D., editors, *The Effects of Noise on Aquatic Life II*, New York, NY. Springer.

Nedwell, J. and Howell, D. (2004). A review of offshore windfarm related underwater noise sources.

Norro, A. M. J., Rumes, B., and Degraer, S. J. (2013). Differentiating between Underwater Construction Noise of Monopile and Jacket Foundations for Offshore Windmills: A Case Study from the Belgian Part of the North Sea. *The Scientific World Journal*, pages 1–7.

Popper, A. N. and Hawkins, A. D., editors (2016). *The Effects of Noise on Aquatic Life II*. Springer, New York, NY.

Popper, A. N. and Hawkins, A. D. (2018). The importance of particle motion to fishes and invertebrates. *The Journal of the Acoustical Society of America*, 143(1):470–488.

Popper, A. N., Hawkins, A. D., Fay, R. R., Mann, D. A., Bartol, S., Carlson, T. J., Coombs, S., Ellison, W. T., Gentry, R. L., Halvorsen, M. B., Løkkeborg, S., Rogers, P. H., Southall, B. L., Zeddies, D. G., and Tavolga, W. N. (2014). *Sound Exposure Guidelines for Fishes and Sea Turtles: A Technical Report prepared by*

ANSI-Accredited Standards Committee S3/SC1 and registered with ANSI. ASA S3/SC1.4 TR-2014. Springer International Publishing, Cham, Switzerland.

Robinson, S. P. and Theobald, P. (2017). A Standard for the Measurement of Underwater Sound Radiated from Marine Pile Driving. *24th International Congress on Sound and Vibration*.

Sigray, P. and Andersson, M. H. (2011). Particle motion measured at an operational wind turbine in relation to hearing sensitivity in fish. *The Journal of the Acoustical Society of America*, 130.

Southall, B. L., Finneran, J. J., Reichmuth, C., Nachtigall, P. E., Ketten, D. R., Bowles, A. E., Ellison, W. T., Nowacek, D. P., and Tyack, P. L. (2019). Marine Mammal Noise Exposure Criteria: Updated Scientific Recommendations for Residual Hearing Effects. *Aquatic Mammals*, 45(2):125–232.

Tetra Tech (2012). Block Island Wind Farm and Block Island Transmission System Environmental Report / Construction and Operations Plan. Technical report, Submitted by Deepwater Wind, Boston, MA.

Topham, E., Gonzalez, E., McMillan, D., and João, E. (2019). Challenges of decommissioning offshore wind farms: Overview of the European experience. In *Journal of Physics: Conference Series*, volume 1222.

Tougaard, J., Henriksen, O. D., and Miller, L. A. (2009). Underwater noise from three types of offshore wind turbines: Estimation of impact zones for harbor porpoises and harbor seals. *The Journal of the Acoustical Society of America*, 125(6):3766–3773.

Tsouvalas, A. and Metrikine, A. V. (2016). Structure-Borne Wave Radiation by

Impact and Vibratory Piling in Offshore Installations : From Sound Prediction to Auditory Damage. *Journal of Marine Science and Engineering*.

US Department of Energy (2016). National offshore wind strategy - facilitating the development of the offshore wind industry in the US. Technical report, US Department of Energy.

Vigness-Raposa, K. J., Giard, J. L., Frankel, A. S., Miller, J. H., Potty, G. R., Lin, Y.-T., Newhall, A. E., and Mason, T. (2017). Variations in the acoustic field recorded during pile-driving construction of the Block Island Wind Farm. *The Journal of the Acoustical Society of America*, 141.

Wilkes, D. R. and Gavrilov, A. N. (2017). Sound radiation from impact-driven raked piles. *Journal of the Acoustical Society of America*, 142(1):1–11.

Wind Europe (2018). Offshore wind in Europe. Technical report, Wind Europe.

Wu, X., Hu, Y., Li, Y., Yang, J., Duan, L., Wang, T., Adcock, T., Jiang, Z., Gao, Z., Lin, Z., Borthwick, A., and Liao, S. (2019). Foundations of offshore wind turbines: A review. *Renewable and Sustainable Energy Reviews*, 104:379–393.

MANUSCRIPT 2

Characterization of impact pile driving signals during installation of offshore wind turbine foundations

This manuscript was written for publication in the Journal of the Acoustical Society of America as part of a special issue on The Effects of Noise on Aquatic Life. It was accepted for publication on March 19, 2020 and published online on April 17, 2020.

Amaral, J. L., Miller, J. H., Potty, G. R., Vigness-Raposa, K. J., Frankel, A. S., et al. (2020). Characterization of impact pile driving signals during installation of offshore wind turbine foundations. The Journal of the Acoustical Society of America, 147(4), 2323-2333. https://doi.org/10.1121/10.0001035.

Jennifer L. Amaral, James H. Miller and Gopu R. Potty

Department of Ocean Engineering, University of Rhode Island, Narragansett, RI 02882, USA

Kathleen J. Vigness-Raposa and Adam S. Frankel

Marine Acoustics, Inc, 2 Corporate Place, Suite 105, Middletown, RI 02842, USA

Ying-Tsong Lin and Arthur E. Newhall

Applied Ocean Physics and Engineering, Woods Hole Oceanographic Institution, Woods Hole, MA 02543, USA

Daniel R. Wilkes and Alexander N. Gavrilov

Centre for Marine Science and Technology, School of Earth and Planetary Sciences, Curtin University, GPO Box U1987, Perth, Western Australia 6845, Australia

Abstract: Impact pile driving creates intense, impulsive sound that radiates into the surrounding environment. Piles driven vertically into the seabed generate an azimuthally symmetric underwater sound field whereas piles driven on an angle will generate an azimuthally dependent sound field. Measurements were made during pile driving of raked piles to secure jacket foundation structures to the seabed in waters off the northeastern coast of the U.S. at ranges between 500 m and 15 km. These measurements were analyzed to investigate variations in rise time, decay time, pulse duration, kurtosis, and sound received levels as a function of range and azimuth. Variations in the radiated sound field along opposing azimuths resulted in differences in measured sound exposure levels of up to 10 dB and greater due to the pile rake as the sound propagated in range. The raked pile configuration was modeled using an equivalent axisymmetric FEM model to describe the azimuthally dependent measured sound fields. Comparable sound level differences in the model results confirmed that the azimuthal discrepancy observed in the measured data was due to the inclination of the pile being driven relative to the receiver.

2.1 Introduction

Impact pile driving creates intense sound that radiates into the environment and propagates through the air, water, and sediment. Characteristics of the resulting sound radiation are strongly dependent on the pile configuration, hammer impact energy, and environmental properties at the pile location and in the surrounding area. With the development of offshore wind farms globally there have been increased opportunities to measure the underwater sound fields generated during pile driving activities in different environments and of varying pile diameters (Göttsche et al., 2015; Robinson et al., 2012; Bailey et al., 2010; De Jong and Ainslie, 2008; Norro et al., 2013). The majority of these measurements have been of monopiles or other vertically driven piles, while few measurements of raked (angled) piles have been described (Wilkes and Gavrilov, 2017; Martin and Barclay, 2019).

The dominant source of sound that is generated during pile driving is due to the hammer impact. For a hollow steel pile, the resulting sound field is comprised of a series of Mach waves (Reinhall and Dahl, 2011; Dahl and Dall'Osto, 2017; Dahl and Reinhall, 2013; Zampolli et al., 2013). The hammer strike and resulting compression wave cause the pile to bulge outwards and deform, due to the Poisson effect. This physical deformation propagates down the pile and acts as a moving sound source. The resulting acoustic field consists of a series of downward- and upward-propagating axisymmetric Mach wave cones (Kim et al., 2013; Reinhall and Dahl, 2011).

Reinhall and Dahl (2011) and Kim et al. (2013) described the propagation of these Mach wave cones from vertically driven piles, and Wilkes and Gavrilov (2017) modeled the Mach cone radiating from an angled pile. The angle of the initial Mach cone relative to the pile axis is dependent on the ratio of the sound

speed in water (c_w) to the propagation speed of the radial deformation down the pile (c_p), which is close to the compressional wave speed in steel (Equation 2.1; Reinhall and Dahl, 2011).

$$\theta = sin^{-1}(c_w/c_p) \tag{2.1}$$

Raked piles are common in infrastructure projects because of their increased resistance to lateral loads. Due to the non-axisymmetric geometry of the pile relative to the seabed, raked piles are expected to radiate underwater sound with an azimuthal dependence. Wilkes and Gavrilov (2017) and Martin and Barclay (2019) demonstrated that sound radiation from a raked pile is significantly different at various azimuths from the pile. Measured sound exposure levels (SELs) radiated by piles raked at an angle of 14° to the vertical and inclined towards the receiver were 10 dB lower at distances of 1.2-1.5 km than those radiated from piles inclined away from the receiver (Wilkes and Gavrilov, 2017).

The sounds generated from impact pile driving are described as impulsive, which exhibit physical characteristics at the source that make them potentially more injurious to marine mammals and fishes as compared to non-impulsive sounds (Southall et al., 2019; Popper et al., 2014). Impulsive signals are defined as short-duration broadband sounds that consist of a peak sound pressure amplitude with a rapid rise time to the peak followed by a decay (National Marine Fisheries Service, 2018). An impulsive signal may undergo changes due to propagation effects that could result in the signal being perceived by animals as non-impulsive at some other range (Southall et al., 2007, 2019; National Marine Fisheries Service, 2018). A range at which a signal might transition from being considered impulsive to non-impulsive was briefly identified as 3 km in draft sound exposure guidance, but was omitted from the final guidance as more research is needed to determine

this range (National Marine Fisheries Service (NMFS), 2015). The consideration of a transition range is important when applying acoustic exposure guidance as Southall et al. (2019) recommends that the signal characteristics expected to be received by the animal rather than those at the source dictate the exposure guidance used (impulsive or non-impulsive). Since propagation is dependent on the local environmental conditions (sound speed, bottom sediment properties, water depth, surface roughness, etc.), defining a definitive distance that would be valid for all propagation environments is not straightforward. Also, what measurable signal characteristic could be used to determine when a signal has undergone that transition?

One such metric could be kurtosis, which is a statistical measure that represents the impulsiveness of an event (National Marine Fisheries Service, 2018). According to Hamernik et al. (2003) and Lei et al. (1994), the kurtosis of a signal, in addition to an energy metric, is an important variable in determining hazards to hearing and is a good predictor of the relative magnitude of acoustic trauma between signals that differ in impulsiveness. Impulsive signals with high kurtosis and high instantaneous peak sound pressure may be more injurious to certain mammals (Southall et al., 2007). Rise time is another relevant metric to describe the temporal structure of the signal that could be tied to the impact a sound will have (Henderson and Hamernik, 1986; Laughlin, 2005). Studies are ongoing to determine the most appropriate metric, but the onset of damage to hearing for impulsive sounds may be more appropriately measured by the rise time of a signal as opposed to the kurtosis (Popper et al., 2006). Additionally, a combination of the rise time, ratio of peak pressure to pulse duration, pulse duration, and crest factor could all be metrics used to evaluate a change in the impulsive nature of a signal over range (Hastie et al., 2019).

This study will present measurements collected from the installation of raked piles in coastal waters at the Block Island Wind Farm (BIWF) off the coast of Block Island, Rhode Island, USA. Steel piles were driven into the seabed to pin the jacket-type wind turbine foundation structures at BIWF. These types of foundations were used due to their suitability in deeper waters relative to other foundations currently available. Jacket foundations have been used extensively in the offshore oil and gas industry and were a cost-effective choice for the BIWF based on the robust supply chain in the U.S for the construction and installation of these foundations. Based on these factors, the jacket foundation was the preferred choice for the BIWF (Tetra Tech, 2012).

The piles driven at the BIWF were raked at an angle of 13.27° to the vertical. This rake resulted in the incident angle of the radiated Mach wave on the seabed changing based on azimuth. The Mach wave generated with each hammer strike is radiated out from the pile at an angle typically around 18° depending on the exact ratio of the speed of sound in steel and the surrounding water (MacGillivray, 2018; Dahl and Dall'Osto, 2017). The similarities between the pile rake and Mach wave angle resulted in the sound radiating from the pile axis in the direction of the pile inclination to be directed more towards the seafloor as opposed to the sound in the opposite direction which was directed near horizontal into the water column. The steeper the incident angle of the Mach wave to the seafloor, the more energy was absorbed by the seafloor (HDR, 2018). The effect of pile rake on the resulting sound field was evident in the received signals. This sound radiation pattern is demonstrated in Wilkes and Gavrilov (2017) where the pile orientation is similar to that of the BIWF.

The objective of this study was to describe the measurements collected of pile driving at the BIWF as a function of range, azimuth, and strike energy. The

variation in the rise time, decay time, pulse duration, and kurtosis of the signals was investigated to determine if there was supporting evidence to define a range at which the signal transitioned from impulsive to non-impulsive. Martin and Barclay (2019) presented measurements of pile driving at BIWF from stationary systems and analyzed the data using linear mixed models based on damped cylindrical spreading to conclude that the variability in the received level was largely due to the pile rake. The study described in this manuscript utilizes a finite element model to investigate the variation observed in the data from both towed and stationary systems to further explain the conclusion that the dominant source of the sound level variation was the inclination of the pile relative to the receiver.

The paper is organized in the following manner. Section II describes the study location along with the measurement equipment, details of the turbine foundations and piling activity, and analysis methods. Section III presents the data collected and the variations observed in the measured sound levels due to the pile rake and range. The pulse duration and kurtosis of the pile driving signals are also discussed. Section IV includes a discussion of the observations as compared to modeled results. Section V presents the main conclusions of this study.

2.2 Observation Methods

The location of the following study was the Block Island Wind Farm, which is the first offshore wind farm in U.S. waters. It is a 30-megawatt wind farm that is comprised of five 6-MW turbines located three miles southeast of Block Island, Rhode Island in water depths of approximately 30 meters. The U.S. Bureau of Ocean Energy Management (BOEM) funded a project to study the development and operation of this wind farm. The goal of the project was to collect real-time measurements of the construction and operation activities from the first federally permitted offshore wind farm in U.S. coastal waters to allow for more accurate

assessments of the environmental effects and inform development of appropriate mitigation measures.

The University of Rhode Island (URI), Marine Acoustics, Inc. (MAI) and Woods Hole Oceanographic Institution (WHOI) were funded under this project to investigate the acoustic pressure and particle velocity associated with the construction and operation of the wind turbines. Various stationary and towed acoustic measurement systems were deployed (Figure 2.1) in the vicinity of the BIWF. The measurements collected on the stationary and towed systems during the pile driving activities that occurred between September and October of 2015 were analyzed and will be discussed in this paper. Measurements were made at ranges between 500 m and 15 km from the wind turbine foundations.

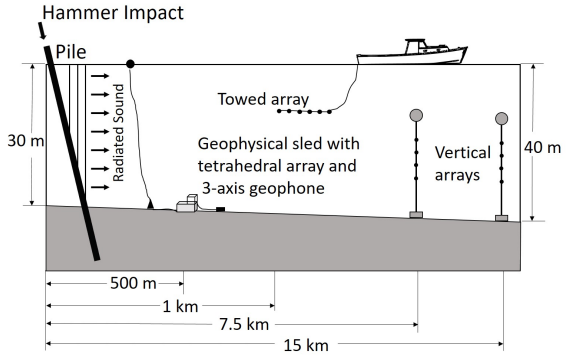

Figure 2.1. Simplified schematic of all the measurement systems deployed by URI, MAI, and WHOI to measure the underwater sound and particle velocity generated by the pile driving associated with the Block Island Wind Farm (BIWF).

2.2.1 Measurement Equipment

Stationary measurement systems of two vertical line arrays (VLAs) and a bottom-deployed geophysical sled were deployed for 24 days between October and November 2015. Pile driving on seven separate days was recorded during this deployment. Data were recorded continuously on sensors connected to Several

Hydrophone Receive Units (SHRUs) developed and maintained by WHOI. All of the sensors were recording at a sampling rate of approximately 10 kHz for the duration of the deployment.

A geophysical sled that included a four-hydrophone tetrahedral array and a geophone sensor package was deployed 500 m from the foundation of the Wind Turbine Generator (WTG) 3 in roughly 26 m of water. The sensor package consisted of a three-axis geophone and a low sensitivity hydrophone. Acoustic particle velocity was measured in the water column and on the seabed using the tetrahedral array and the geophone data. The hydrophones used in the array were the HTI-94-SSQ model from High Tech, Inc with a sensitivity of -204 dB re 1V/μPa. They were spaced 0.5 m apart in the array and deployed at the seafloor.

The two vertical line arrays each consisted of four HTI-94-SSQ hydrophones spaced 5 m apart at water depths between 20-40 m. Two different amplifier gains were applied to the signals recorded on the array. The sensitivity of these hydrophones was -170 dB re 1V/μPa. One of the amplifier gain settings resulted in the pressure signals being clipped and therefore these data were eliminated from the analysis and only the non-clipped data were used. These arrays were moored 7.5 km and 15 km from the WTG 3 location and were both in roughly 40 m of water (Figure 2.2).

In addition to the stationary sensors, a passive towed array was deployed by MAI on two separate days from the R/V *Shanna Rose* during pile driving to measure the received sound levels with range from the foundation. The array consisted of eight elements irregularly spaced over its 120 m length. Approximately 50 m of lead-in cable was deployed to keep the array at depths between 6 and 12 m during the pile driving. Sea Bird SBE39 temperature and pressure sensors were placed along the array cable to estimate the shape of the array in the water column

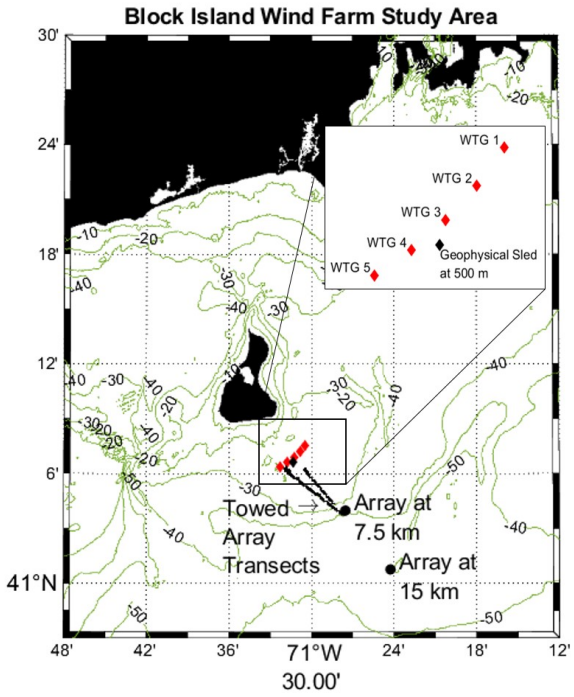

Figure 2.2. Location of the vertical line arrays at 7.5 km and 15 km from the Wind Turbine Generator (WTG) foundations and the geophysical sled at 500 m. The two towed array transects are also shown. Bottom depth contours are indicated in meters.

during deployment.

When towing the array, the vessel maintained a linear course away from the foundations at a speed of approximately 1.5 m/s out to distances of 6 and 8 km on the two days. The maximum distance was dictated by the duration of the pile driving activity on both days. Data at ranges greater than 5 km were eliminated from this analysis due to decreasing signal-to-noise ratio in the recorded data. The noise was due to flow-induced turbulent pressure fluctuations on the hydrophones. The analog output from the array was low pass filtered at 30 kHz and amplified with an Alligator Technologies SCS-820 filter board. A National Instruments PCI-6071E card digitized the filtered data at a sampling rate of 64 kHz. Amplifier gains were applied during data acquisition to increase the signal amplitude as the

range of the array from the pile driving activity increased. Data were collected using RAVEN Pro v 1.4 (www.birds.cornell.edu/raven) and saved in consecutive 30 second files for post-processing.

2.2.2 Turbine Foundations

The jacket foundations at BIWF consisted of hollow steel tubular members joined together in a lattice structure, which sits on the seabed to support the WTG. The legs of the jacket foundation were raked at an angle of 13.27° to the vertical. Each foundation required cylindrical, steel piles, split into multiple sections, to be impact driven through the legs at the four corners of the structure to secure it to the seabed (Figure 2.3). The diameter of the driven piles was 152 cm with a wall thickness of 4.4 cm. The piles were driven to a depth of up to 76.2 m below the mudline (water-sediment interface) (Tetra Tech, 2012).

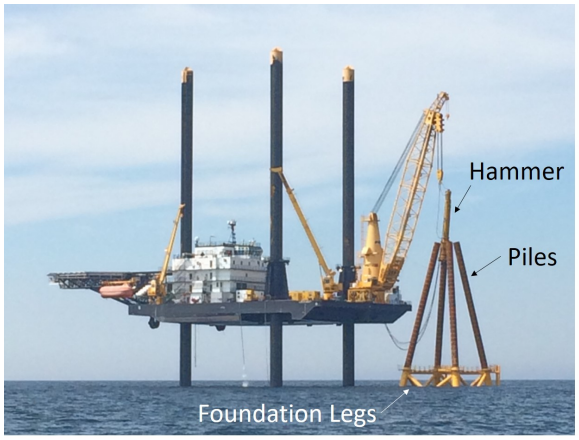

Figure 2.3. Jacket foundation in the water with a pile section inserted into each leg at an angle of 13.27° relative to the vertical and the hammer positioned on one of the piles.

Each foundation had a total of four legs that will be referred to as A1, A2, B1, and B2. Each leg of the foundation required a total of three pile sections, which will be referred to as P1, P2, and P3. Figure 2.4 shows a top-down schematic of the

wind turbine foundation showing the orientation of the four legs and the general direction to the deployed measurement systems in relation to the foundation.

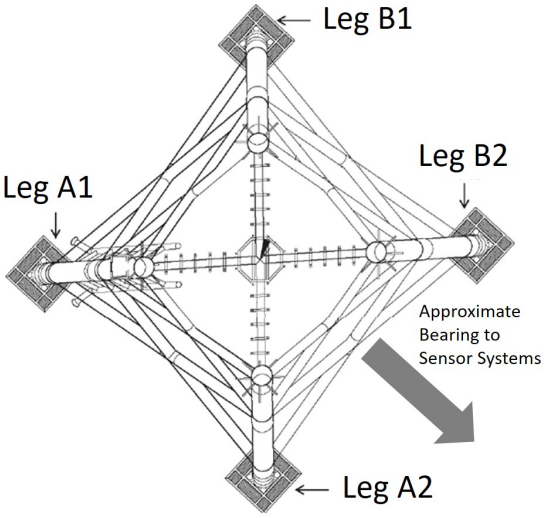

Figure 2.4. Top-down schematic of the jacket foundation showing orientation of the four legs and the direction of the deployed measurement systems in relation to the foundation (Tetra Tech and JASCO, 2015).

The measurement systems deployed during the BIWF construction captured pile driving on various legs and pile sections. No mitigation measures, such as bubble curtains, were employed at BIWF. Due to the location of the measurement systems relative to the foundation, the sound radiated from the piling of legs A1 and B1 was directed towards the seafloor and the sound radiated from the piling of legs A2 and B2 was directed near horizontal into the water column. The effect of pile rake on the resulting sound field was evident in the received signals, with the sound levels from the A2 and B2 legs being higher than those from the A1 and B1 legs.

2.2.3 Data Analysis

Custom analysis scripts were written in MATLAB R2019a (www.mathworks.com) to detect the pile driving signals and evaluate vari-

ous metrics of each recorded hammer strike encompassing the entire recorded frequency range of the signals. The upper limit of the frequency content in the signals recorded on the stationary systems was just under 5 kHz as compared to an upper limit of 30 kHz for the towed array measurements. The peak sound pressure level (SPL_{pk}), sound exposure level (SEL), pulse duration, rise time, decay time, and kurtosis of each individual hammer strike signal were calculated. These measurements were correlated with the strike energy of the hammer to investigate dependence on the initial strike energy and pile orientation. The towed array data were also correlated with distance to investigate the range dependencies of these metrics.

The sound metrics were calculated using the following equations, where $p(t)$ is the sound pressure time series recorded at the receiver.

Peak sound pressure level [dB re 1μPa]:

$$SPL_{pk} = 20 \log_{10} max(|p(t)|) \tag{2.2}$$

The time interval that contains 90% of the sound energy is a meaningful definition of pulse duration for impulsive signals. This energy percentage is defined in the International Organization for Standardization (ISO) 18406 (ISO, 2017b) for the purpose of defining the pulse duration of hammer strikes during impact pile driving. This duration is bounded by the times when the cumulative signal energy exceeds 5% of the total signal energy and ends when it reaches 95% (Southall et al., 2007).

The rise time of a signal is the time it takes for a signal to rise from 10% to 90% of its maximum absolute value of sound pressure, as defined in ISO 10843 (ISO, 1997). The decay time of a signal was calculated as the time it takes for the signal to decay to 95% of the cumulative signal energy from the time of peak sound pressure.

Sound Exposure Level [dB re $1\mu Pa^2s$]: The pulse duration (T) containing 90% of the pulse energy was used to calculate the single strike SEL based on Equation 2.3. All SEL values reported in this paper are single strike values.

$$SEL = 10 \log_{10} \int_T p(t)^2 dt \tag{2.3}$$

Kurtosis is a dimensionless statistical measure of a probability distribution that can be used to describe the shape of an amplitude distribution (Southall et al., 2007). It is the ratio of the fourth central moment divided by the square of the variance of the sound pressure time series over a specified time interval (t_1 to t_2) defined according to Equation 2.4, where $\bar{p}$ is the mean sound pressure within that time interval. This definition is consistent with that presented in ISO 18405 (ISO, 2017a).

$$Kurtosis = \frac{\mu_4}{\mu_2^2} = \frac{\frac{1}{t_2 - t_1} \sum_{t_1}^{t_2} (p(t) - \bar{p})^4}{(\frac{1}{t_2 - t_1} \sum_{t_1}^{t_2} (p(t) - \bar{p})^2)^2} \tag{2.4}$$

While kurtosis can help describe impulsive signals, it is sensitive to variables such as the level and duration of impulses, the temporal structure of the noise, and the duration of the noise sample over which the kurtosis is calculated. Hamernik et al. (2003) reported that the kurtosis stabilized for windows greater than 30 seconds, Lei et al. (1994) calculated kurtosis over a time window of 256 seconds, Martin (2019) recommended calculating kurtosis over a one-minute window, Kastelein et al. (2017) used a one-second time window, and Erdreich (1986) used a time window of 11 seconds. The duration over which to calculate kurtosis is arbitrary, which is highlighted by the varying time duration in the referenced studies. If interest is in marine mammal perception to a certain sound, the time duration could be chosen based on the physiological factors of hearing for a species of interest (Erdreich, 1986).

The purpose of calculating kurtosis on the BIWF data was to use it as a measure of impulsiveness over range based on the temporal structure of the signal of each individual strike. Therefore the kurtosis was calculated for each hammer strike using a one-second window that encompassed the peak in the signal. The window was defined as 0.1 seconds before to 0.9 seconds after the time of the peak. This time window was chosen to contain only one hammer strike.

2.3 Results

The towed array and stationary measurement systems recorded pile driving events along a constant bearing from the jacket foundation, but at varying orientations relative to the raked piles. An event was classified as the pile driving installation of a single pile section. On the stationary vertical line array systems, the installation of sections P2 and P3 for the WTG 1 and 4 foundation legs were recorded, which was a total of 16 pile driving events. On the towed array, two complete pile driving events were recorded for the installation of P1 A2 on WTG 3 and of P1 A1 on WTG 5. The measured sound levels collected on the towed array and vertical line array measurement systems are presented.

All of these measurements were made during the beginning of September through mid-October. While there are seasonal differences in the water temperature and salinity that affect the underwater sound propagation, the time frame of these measurements is concentrated in one season and therefore not expected to result in large differences in the sound propagation. The temperature profiles taken on the days of the towed array transects showed a downward refracting temperature profile that was similar between the two days. Had the pile driving occurred in the winter season, the received SELs at ranges greater than 6 km could have been close to 8 dB higher due to lower water temperature and a more isovelocity sound speed profile (Lin et al., 2019).

2.3.1 Stationary Measurements

The data presented in this paper are from one channel of the vertical line array at 7.5 km from the pile driving activity. They are representative of the data collected on the other channels with similar gain and on the vertical line array at 15 km. This hydrophone was at a depth of 25 m. Figure 2.5 shows the time series of one day of pile driving activity for the installation of section P2 for all four legs on WTG 1. The sound pressure amplitudes of the received signals for the different events are shown, with the amplitudes of events recorded from legs B2 and A2 being much higher than those from legs A1 and B1. These higher amplitudes resulted in the measured SPL_{pk} and SEL for these events being higher than those for the A1 and B1 events (upper two plots of Figure 2.6).

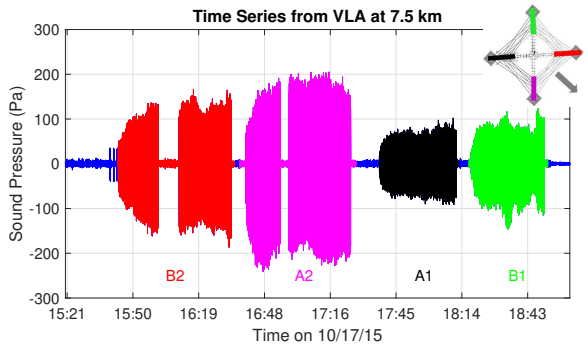

Figure 2.5. Time series example of one day of pile driving on WTG 1 recorded on the array at 7.5 km at a depth of 25 m. The amplitude of the measured pressure signals from the hammer strikes on the B2 and A2 legs are larger than those on the A1 and B1 legs.

To investigate the cause of the differences in received sound pressure amplitudes in Figure 2.5, the strike energy of the individual hammer strikes was correlated to the measured received levels. The pile driving logs were obtained from Menck GmbH (www.menck.com), who was responsible for the pile driving installation for the BIWF. The time records from Menck and the deployed systems were aligned so that the hammer energy associated with each recorded strike could be

compared. This comparison showed that although the measured received sound levels for the driving of legs A2 and B2 were consistently higher, the strike energies used to drive these legs were lower than those used for the driving of legs A1 and B1 (bottom plot in Figure 2.6).

In this example the duration of the piling events for legs A1 and B1 was shorter than the piling of legs A2 and B2. The length of the pile section being driven was the same for all four legs, but the higher strike energy for the duration of the piling for the A1 and B1 legs resulted in the pile reaching depth in a shorter amount of time. During the BIWF construction all pile driving activities had to be completed during daylight hours, ending 30 minutes prior to dusk (Tetra Tech, 2012). It is a reasonable assumption that since legs A1 and B1 were driven last the hammer operators increased the strike energy to ensure the complete installation of these legs before dark. Regardless of the reasoning behind the shorter duration and higher intensity pile driving, the received sound levels were still less than those from legs A2 and B2.

The measured sound levels from the hammer strikes on legs A2 and B2 were consistently higher than those on legs A1 and B1, independent of strike energy during all of the recorded pile driving events (Figure 2.7). This led to the determination that the dominant factor influencing the received sound levels from legs at different azimuths was the inclination of the pile relative to the receiver. Findings presented in Wilkes and Gavrilov (2017) showed a roughly 10 dB difference in SELs received from piles inclined in opposite directions.

2.3.2 Towed Array Measurements

All analysis was performed using the towed array hydrophone farthest from the towing vessel and also the deepest in the water column. It was towed at a depth between 10-12 m during the events. The effect that distance had on the

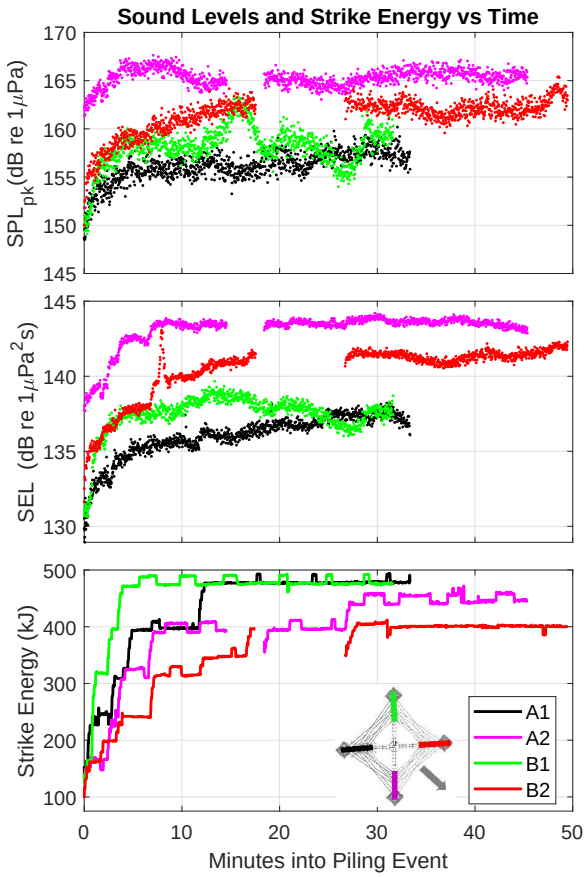

Figure 2.6. Received SPL_{pk} (top), SEL (middle), and corresponding energy (bottom) of the pile driving strikes presented in Figure 2.5. While the strike energy was higher for the piling of legs A1 and B1, the received sound levels were lower for these legs than for legs A2 and B2.

received sound levels and signal characteristics will be presented.

Figure 2.8 shows a comparison of the received sound levels for both of the pile driving events recorded with the towed array. These sound levels have been adjusted to remove the effect of the strike energy by subtracting $10log_{10}(StrikeEnergy)$ from the measured levels, where the strike energy was in kilojoules (kJ). This was done to compare the received levels in relation to the distance from the piling event independent of strike energy. Then the levels were normalized by the maximum received sound level to produce the comparison seen in Figure 2.8. The measured SPL_{pk} and SEL from the piling of leg A2 were con-

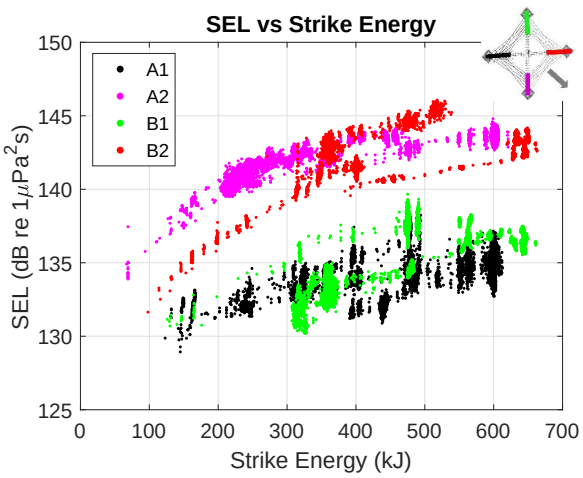

Figure 2.7. SEL versus strike energy for each recorded hammer strike from all 16 measured piling events. The received levels for the piling of legs A2 and B2 were consistently higher than those for legs A1 and B1, independent of strike energy. This supports the determination that the dominant factor influencing the received sound levels from different legs is the inclination of the pile to the receiver.

sistently higher than that of leg A1 over the entire towed array transect, which is thought to be due to the orientation of the leg relative to the receiver.

2.3.3 Variations in Signal Characteristics

The rise and decay time of the signal recorded on the towed array from each hammer strike was calculated and plotted versus distance to investigate its dependence on range from the foundation (Figure 2.9). Only signals with a high enough signal-to-noise ratio to allow for reliable calculation of the rise time were included in the following comparisons. The signals from the A1 leg had longer rise and decay times over range than those from the A2 leg. These differences are thought to be a function of the pile inclination relative to the towed array. Greater seafloor interaction of the sound radiated from the A1 leg resulted in greater time dispersion in the received signal.

Independent of the orientation of the pile, the rise and decay times and the pulse duration of the signals recorded from both legs increased with range as

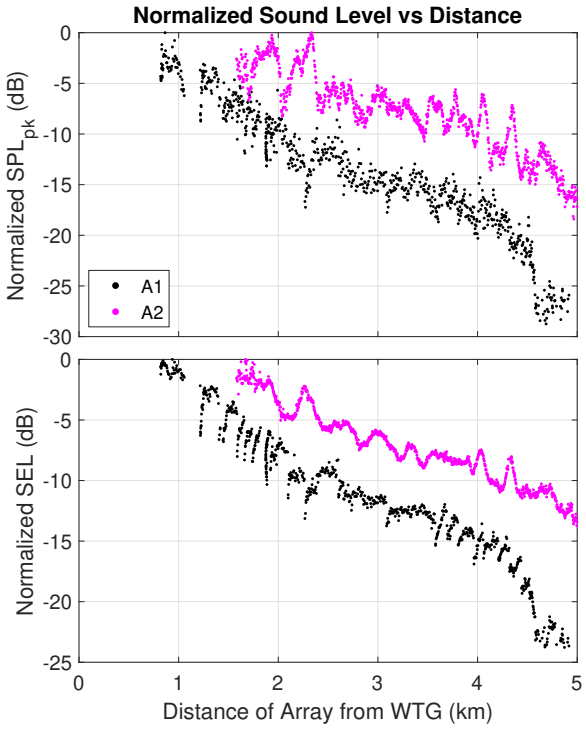

Figure 2.8. Normalized SPL_{pk} (top) and SEL (bottom) versus distance for each hammer strike measured on the towed array for the pile driving of the A2 and A1 legs. Levels have been adjusted to remove the effect of strike energy and normalized to highlight the difference in received levels between the two piling events. The difference increases to around 10 dB by 5 km.

measured by the towed array. The energy in the pulse spreads over time as the signal propagates further in range. These dispersion effects are expected when a broadband acoustic signal is propagated in a shallow water environment (Potty et al., 2003, 2000). Bailey et al. (2010) noted the same trend where there was a decrease in sound level and an increase in pulse duration with increasing distance from the piling.

The pulse duration for each of the signals represented in Figure 2.9 was plotted versus the measured SEL (bottom plot in Figure 2.10). The signals were consistently more spread in time for the piling of leg A1 than for leg A2 based on the propagation paths of the radiated energy. This relationship supports the trend

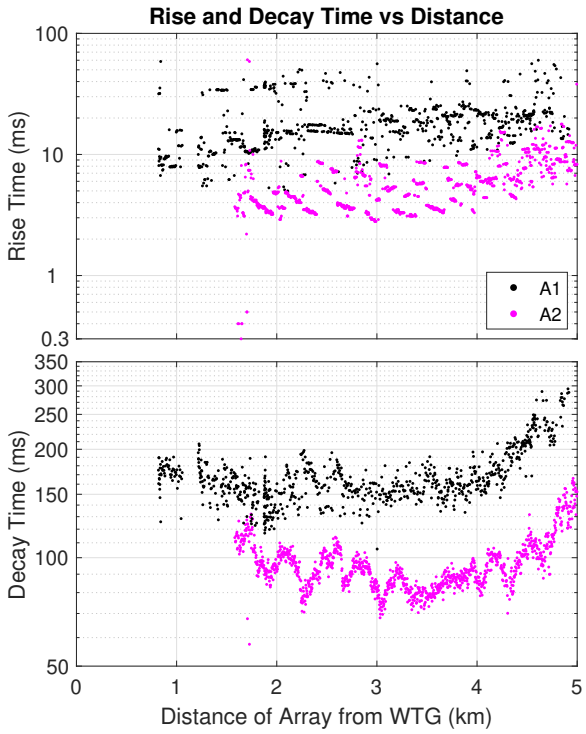

Figure 2.9. Rise time (top) and decay time(bottom) versus distance for each hammer strike measured on the towed array for the pile driving of the A2 and A1 legs. The signal from the A1 leg had longer rise and decay times than the signals recorded from the A2 leg.

seen in the rise and decay time measurements in that the signal becomes more dispersed for higher incident angle propagation.

The top plot in Figure 2.10 shows a similar relationship between the pulse duration and SEL as measured on the vertical line array at 7.5 km for the same piling events seen in Figure 2.5. The pulse duration of the signals received from the A1 and B1 legs is around 200 ms and the received SELs are lower, whereas the pulse duration is around 100 ms with higher received SELs for the A2 and B2 legs. When the radiated sound is directed into the seafloor the signal experiences greater dispersion and attenuation as it propagates out to 7.5 km which results in the received signal energy being spread over a longer time and the received sound pressure amplitude being lower. The higher dispersion is a function of increased

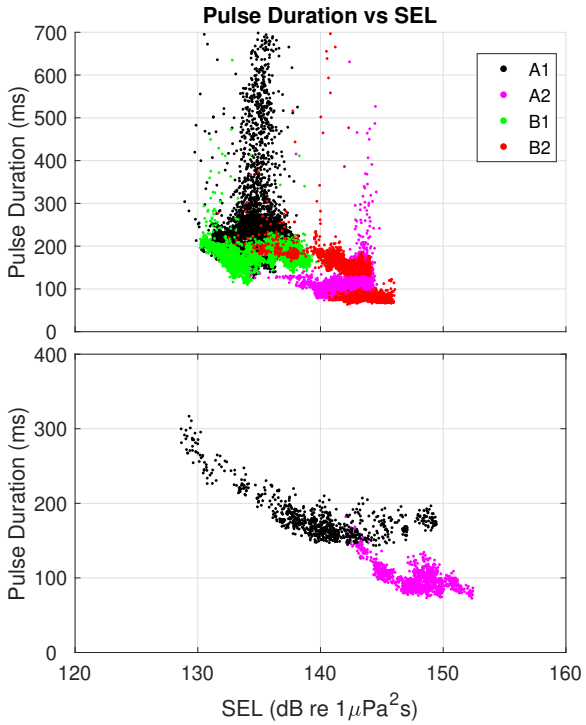

Figure 2.10. Pulse duration versus the measured SEL for each hammer strike recorded on the VLAs (top) and towed array (bottom). The length of the pulse for the piling of leg A1 is consistently longer than that for leg A2, thought to be due to the orientation of the leg.

seafloor interaction that is due to the steeper incident angle of the acoustic wave experienced with the A1 and B1 legs.

2.3.4 Kurtosis

The kurtosis of the recorded signals from the stationary and towed measurement systems was calculated using a one-second time window around each individual hammer strike. The kurtosis calculated on the 7.5 and 15 km stationary array data was similar at both ranges with the average values calculated from the four legs shown in Table 2.1. The kurtosis was slightly lower for the signals from legs A1 and B1 as compared to A2 and B2.

This difference in kurtosis between legs was also seen in the towed array data

shown in Figure 2.11. The higher kurtosis for the A2 leg, in combination with the higher received sound levels and shorter pulse duration, implies that the signals from this leg were more impulsive as compared to those from leg A1. All of these factors can be related to the inclination of the pile relative to the receiver, where the A2 leg oriented away from the receiver experiences less bottom interaction and time dispersion in the propagated signal. The seafloor interaction is greater for the A1 leg and results in a signal with a lower kurtosis and received sound level and a longer pulse duration, which would describe a less impulsive signal.

Table 2.1. Average kurtosis calculated from the hammer strikes related to the piling of each leg recorded on a single channel from the 7.5 and 15 km stationary arrays.

Foundation Leg	Kurtosis at 7.5 km	Kurtosis at 15 km
A1	21.7	20.7
A2	35.6	34.1
B1	23.9	22.3
B2	31.8	26.3

The goal of this analysis was to use kurtosis to characterize the impulsiveness of the signal and determine if there was a range at which the signal could be classified as non-impulsive based on this metric. No clear transition range or threshold were seen in the data presented in Figure 2.11. In order to define a range at which the signal transitions, a threshold would need to be defined below which a signal could be considered non-impulsive. Without a clear threshold to compare against, the measurements in Figure 2.11 show that the signals from leg A2 have higher kurtosis and could be considered more impulsive relative to the signals received from leg A1 over the same range.

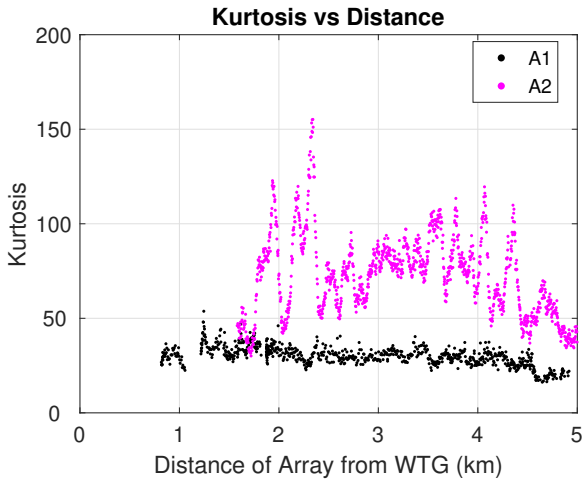

Figure 2.11. Kurtosis versus distance calculated over a one-second time window around each individual hammer strike recorded on the towed array.

2.4 Discussion

The sound radiation from the raked BIWF piles was modeled to validate the underlying physics influencing the trends in the measured data. The modeled results were compared to the measurements from the towed array to explain the azimuthally dependent variations observed in the data. A detailed model-data comparison was not performed due to insufficient detail of the hammer parameters to inform the modeled source forcing function. Pile driving analyzer (PDA) measurements would normally be used to validate the source force function used in modeling but were not available for the BIWF project. This detailed comparison could be undertaken as part of a future modeling effort but was not the focus of the study presented in this paper.

The BIWF piles were modeled using an equivalent inclined vertical array numerical modeling approach. In this model the near-field Green's function was calculated using an axisymmetric FEM model of a vertical pile. The Green's function in the context of this modeling is the complex sound pressure field versus frequency, depth, and range that results from a unit-amplitude harmonic force

applied to the top of a modeled pile (Wilkes and Gavrilov, 2017). The FEM modeled the Green's function at a reference distance of about 6 m from the pile, which was simulated by a line array of point sources placed along the axis of the vertical pile, as detailed in Wilkes and Gavrilov (2017). The vertical array consisted of 100 equidistant spaced point sources placed along the array axis from 0.19 m below the sea surface to 37.81 m near the pile foot, with 0.38 m spacing. To represent a raked pile, the vertical line array was rotated by the angle of pile incline to align the axis of the modeled array with that of the raked pile. The sound field was then propagated into the sediment and water column using a wavenumber integration underwater sound propagation model (Jensen et al., 2011). The modeling approach is described in more detail in Wilkes and Gavrilov (2017).

The pile configuration and environmental characteristics of the BIWF study area (Table 2.2) were used as inputs to calculate the Green's function. All other modeling parameters of the raked-pile configuration used to represent BIWF were the same as those described in Wilkes and Gavrilov (2017). The steel pile density, Young's modulus, and Poisson's ratio, along with the sand seabed and water column density and sound speed were consistent with that in the referenced paper.

Table 2.2. Input parameters used in the numerical modeling approach to describe the BIWF scenario.

Pile Parameters	Length	L	62.5 m
	Diameter	D	1.52 m
	Wall thickness	t	44.45 mm
	Penetration depth		14 m
	Inclination Angle	θ	13.27°
Environmental Parameters	Water depth	d_w	24 m

One half of the space surrounding the pile was modeled due to the symmetry of the pile orientation in the water column and seabed. This resulted in seven

azimuth angles between 0° and 180° being modeled in 30° increments. The model was computed on a frequency grid from 10 Hz to 2000 Hz in 1 Hz increments to encompass the frequency bands with the majority of the sound energy measured from BIWF. The coupling range of the sound field model to be propagated to longer ranges from the inclined vertical array was 20 m.

The Green's function of the raked pile in the underwater sound channel was calculated at a range of 20 m, for 200 receiver depths ranging between 0.38 m to 76 m at increments of 0.38 m, and for seven azimuths. The modeled azimuth of 30° is in the direction of pile incline where the radiated sound is directed towards the seafloor (as measured with leg A1) as opposed to the azimuth of 150° which is in the direction opposite the pile incline where the radiated sound is directed through the water column (as measured with leg A2). The magnitude of the Green's functions calculated at a range of 20 m for azimuths of 30° and 150° is shown in Figure 2.12. The differences between the sound radiated along each azimuth are highlighted in the figure. The magnitude of the radiated sound is greater near the seafloor along the 30° azimuth as compared to the 150° azimuth.

The combined effect that the depth, frequency, and azimuth dependent differences have on the propagation of the pile driving signal over range was investigated by utilizing the ORCA normal mode model (Westwood et al., 1996). This algorithm was used to propagate the Green's function estimated at 20 m out to a range of 3 km. The modeled SEL was similar along the two azimuths out to a range of around 300 m, after which the SEL along the 150° azimuth (radiated sound directed through water column) was greater than that along the 30° azimuth (radiated sound directed at seafloor) (Figure 2.13).

The modeled sound fields were compared to the measurements from the towed array to validate the fall-off and azimuthal discrepancies observed in the data. The

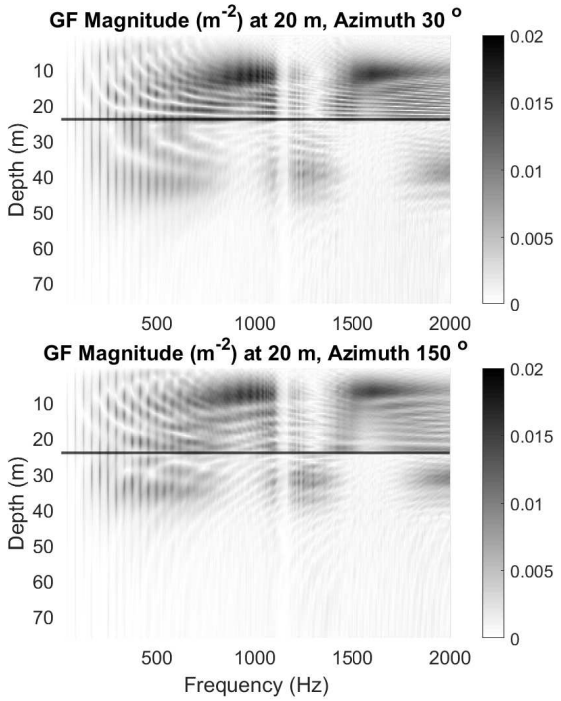

Figure 2.12. Modeled Green's function (GF) magnitude at 20 m range from the raked pile at azimuths of 30° (top) and 150° (bottom) to correspond to the azimuths of the towed array transects during the leg A1 and A2 pile driving events, respectively. The line at a depth of 24 meters represents the modeled seafloor.

measured data were adjusted to remove the effect of strike energy as described in Section III.B. Modeled SEL at azimuths of 30° and 150° at a depth of 12 m, which corresponds to the depth of the towed array, were compared to the adjusted measured SEL during the piling events. The modeled and adjusted measured values were normalized to highlight the differences in levels along the two azimuths (Figure 2.13).

The model results predict azimuthal differences in the resulting sound field from the piling of a raked pile. These differences increase to more than 10 dB as the range increases due to the vertical directionality of the sound source at different azimuth angles. A detailed comparison of the model results to the measured levels will be undertaken as a further study.

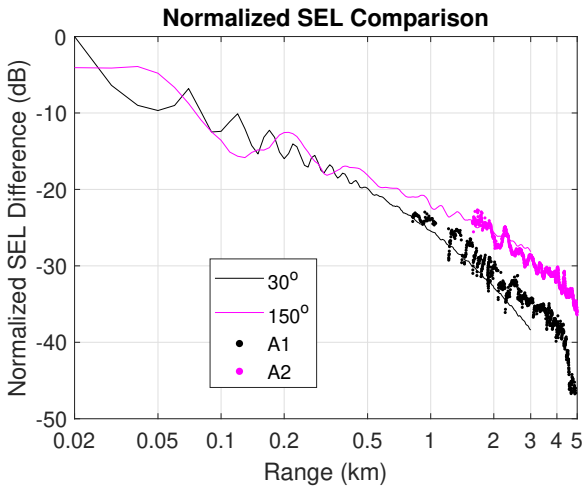

Figure 2.13. Comparison between the measured data (adjusted for strike energy and normalized) on the towed array and the normalized modeled data along the 30° and 150° azimuths. Differences in SEL of approximately 10 dB are observed at a range of 3 km.

2.5 Conclusions

The dominant factor influencing the received sound levels from the installation of raked piles via impact pile driving was the inclination of the pile being driven relative to the receiver. The jacket foundation at BIWF required piles to be driven on an angle of 13.27° and the received sound levels and measured signal characteristics exhibited azimuthal dependence. The rake of the pile directed the radiated sound towards the seafloor in the direction of the pile incline (as with legs A1 and B1) and near horizontally in the direction opposite the pile incline (as with legs A2 and B2). The azimuthal discrepancy observed in the measurements collected at BIWF was due to the raked piles in the foundation.

Sound levels differences of 5-10 dB were observed for piles inclined in opposite directions. The magnitude and trend of the azimuthal discrepancies in sound level were explained with the model results. More detailed modeling and comparison to measured results will be a focus of further study.

The kurtosis demonstrated that the signals received along azimuths in the

direction of pile incline were less impulsive than the signals received along the azimuths opposite the pile incline. This was consistent with the rise and decay time and pulse duration of the signals being longer when the energy was radiated more towards the seafloor as opposed to through the water column. The kurtosis decreased, while the rise time, decay time, and pulse duration increased, with range from the piling activity as the signal became more dispersed and less impulsive. Additional analysis is needed to determine which metrics and thresholds most reliably describe when a signal transitions from being considered impulsive to non-impulsive. This information would be beneficial when assessing sound exposure on marine animals and determining the best exposure criteria to use.

The azimuthal variability in the sound field is an important factor to consider for noise mitigation and environmental assessments that are performed for raked pile installations. Environmental assessments determine the range to different acoustic thresholds enforced by federal regulations. The azimuthally dependent sound fields from a raked pile installation will impact those ranges. This will result in the mitigation range being larger along azimuths closer to 180° as opposed to those along azimuths closer to 0° measured along the pile axis relative to a receiver.

Acknowledgments: This paper was presented at the fifth International Meeting on The Effects of Noise on Aquatic Life held in Den Haag, July 2019. Study concept, oversight, and funding for the experiment were provided by the U.S. Department of the Interior, Bureau of Ocean Energy Management (BOEM), Environmental Studies Program, Washington, DC under Contract Number M15PC00002, Task Order M16PD00025. Collaborators in this project include Randy Gallien and Anwar Khan (HDR, Inc.).

Bibliography

Bailey, H., Senior, B., Simmons, D., Rusin, J., Picken, G., and Thompson, P. M. (2010). Assessing underwater noise levels during pile-driving at an offshore windfarm and its potential effects on marine mammals. *Marine Pollution Bulletin*, 60(6):888–897.

Dahl, P. H. and Dall'Osto, D. R. (2017). On the underwater sound field from impact pile driving: Arrival structure, precursor arrivals, and energy streamlines. *The Journal of the Acoustical Society of America*, 142(2):1141–1155.

Dahl, P. H. and Reinhall, P. G. (2013). Beam forming of the underwater sound field from impact pile driving. *The Journal of the Acoustical Society of America*, 134(1).

De Jong, C. and Ainslie, M. A. (2008). Underwater radiated noise due to the piling for the Q7 Offshore Wind Park. In *The Journal of the Acoustical Society of America*, volume 123.

Erdreich, J. (1986). A distribution based definition of impulse noise. *Journal of the Acoustical Society of America*, 79(4):990–998.

Göttsche, K. M., Steinhagen, U., and Juhl, P. M. (2015). Numerical evaluation of pile vibration and noise emission during offshore pile driving. *Applied Acoustics*, 99:51–59.

Hamernik, R. P., Qiu, W., and Davis, B. (2003). The effects of the amplitude distribution of equal energy exposures on noise-induced hearing loss: The kurtosis metric. *The Journal of the Acoustical Society of America*, 114(1):386–395.

Hastie, G., Merchant, N. D., Götz, T., Russell, D. J. F., Thompson, P., and Janik, V. M. (2019). Effects of impulsive noise on marine mammals: investigating range dependent risk. *Ecological Applications*.

HDR (2018). Field Observations During Wind Turbine Foundation Installation at the Block Island Wind Farm, Rhode Island Appendix D: Underwater Sound Monitoring Reports.

Henderson, D. and Hamernik, R. P. (1986). Impulse Noise: Critical Review. *Journal of the Acoustical Society of America*, 80(2):569–584.

ISO (1997). *ISO 10843 Acoustics - Methods for the description and physical measurement of single impulses or series of impulses*. International Organization for Standardization, Geneva, Switzerland.

ISO (2017a). *ISO 18405 Underwater Acoustics - Terminology*. International Organization for Standardization, Geneva, Switzerland.

ISO (2017b). *ISO 18406 Underwater acoustics â€" Measurement of radiated underwater sound from percussive pile driving*. International Organization for Standardization, Geneva, Switzerland.

Jensen, F. B., Kuperman, W. A., Porter, M. B., and Schmidt, H. (2011). *Computational Ocean Acoustics*. Springer Science, New York, NY, second edition.

Kastelein, R. A., Helder-Hoek, L., Van de Voorde, S., von Benda-Beckmann, A. M., Lam, F.-P. A., Jansen, E., de Jong, C. A. F., and Ainslie, M. A. (2017). Temporary hearing threshold shift in a harbor porpoise (Phocoena phocoena) after exposure to multiple airgun sounds. *The Journal of the Acoustical Society of America*, 142(4):2430–2442.

Kim, H., Miller, J. H., and Potty, G. R. (2013). Predicting underwater radiated noise levels due to the first offshore wind turbine installation in the U.S. *Proceedings of Meetings on Acoustics*, 19:040067.

Laughlin, J. (2005). Underwater Sound Levels Associated With Pile Driving on the Sr 24 , I-82 To Keys Road Project â€“ Yakima River. Technical Report July, Washington State Department of Transportation.

Lei, S., Ahroon, W. A., and Hamernik, R. P. (1994). The application of frequency and time domain kurtosis to the assessment of hazardous noise exposures. *The Journal of the Acoustical Society of America*, 95(5):3005–3005.

Lin, Y.-T., Newhall, A. E., Miller, J. H., Potty, G. R., and Vigness-Raposa, K. J. (2019). A three-dimensional underwater sound propagation model for offshore wind farm noise prediction. *The Journal of the Acoustical Society of America*, 145(5):EL335–EL340.

MacGillivray, A. (2018). Underwater noise from pile driving of conductor casing at a deep-water oil platform. *The Journal of the Acoustical Society of America*, 143(1):450–459.

Martin, S. B. (2019). *One minute at a time: Advancing our ability to estimate effects of man-made sound on marine life*. PhD thesis, Dalhousie University Halifax, Nova Scotia.

Martin, S. B. and Barclay, D. R. (2019). Determining the dependence of marine pile driving sound levels on strike energy , pile penetration , and propagation effects using a linear mixed model based on damped cylindrical spreading. *The Journal of the Acoustical Society of America*, 146(1):109–121.

National Marine Fisheries Service (2018). 2018 Revision to: Technical Guidance for Assessing the Effects of Anthropogenic Sound on Marine Mammal Hearing (Version 2.0): Underwater Thresholds for Onset of Permanent and Temporary Threshold Shifts. Technical report, U.S. Department of Commerce, NOAA.

National Marine Fisheries Service (NMFS) (2015). DRAFT Guidance for Assessing the Effects of Anthropogenic Sound on Marine Mammal Hearing. Technical report, U.S. Department of Commerce.

Norro, A. M. J., Rumes, B., and Degraer, S. J. (2013). Differentiating between Underwater Construction Noise of Monopile and Jacket Foundations for Offshore Windmills: A Case Study from the Belgian Part of the North Sea. *The Scientific World Journal*, pages 1–7.

Popper, A. N., Carlson, T. J., Hawkins, A. D., Southall, B. L., and Gentry, R. L. (2006). Interim Criteria for Injury of Fish Exposed to Pile Driving Operations : A White Paper.

Popper, A. N., Hawkins, A. D., Fay, R. R., Mann, D. A., Bartol, S., Carlson, T. J., Coombs, S., Ellison, W. T., Gentry, R. L., Halvorsen, M. B., Løkkeborg, S., Rogers, P. H., Southall, B. L., Zeddies, D. G., and Tavolga, W. N. (2014). *Sound Exposure Guidelines for Fishes and Sea Turtles: A Technical Report prepared by ANSI-Accredited Standards Committee S3/SC1 and registered with ANSI. ASA S3/SC1.4 TR-2014*. Springer International Publishing, Cham, Switzerland.

Potty, G. R., Miller, J. H., and Lynch, J. F. (2003). Inversion for sediment geoacoustic properties at the New England Bight. *The Journal of the Acoustical Society of America*, 114(4):1874–1887.

Potty, G. R., Miller, J. H., Lynch, J. F., and Smith, K. B. (2000). Tomographic

inversion for sediment parameters in shallow water. *The Journal of the Acoustical Society of America*, 108(3):973–986.

Reinhall, P. G. and Dahl, P. H. (2011). Underwater Mach wave radiation from impact pile driving: Theory and observation. *The Journal of the Acoustical Society of America*, 130(3):1209–1216.

Robinson, S. P., Theobald, P. D., and Lepper, P. A. (2012). Underwater noise generated from marine piling. *Proceedings of Meetings on Acoustics*, 17.

Southall, B. L., Bowles, A. E., Ellison, W. T., Finneran, J. J., Gentry, R. L., Greene Jr, C. R., Kastak, D., Ketten, D. R., Miller, J. H., Nachtigall, P. E., Richardson, W. J., Tomas, J. A., and Tyack, P. L. (2007). Marine Mammal Noise Exposure Criteria: Initial Scientific Recommendations. *Aquatic Mammals*, 33(4).

Southall, B. L., Finneran, J. J., Reichmuth, C., Nachtigall, P. E., Ketten, D. R., Bowles, A. E., Ellison, W. T., Nowacek, D. P., and Tyack, P. L. (2019). Marine Mammal Noise Exposure Criteria: Updated Scientific Recommendations for Residual Hearing Effects. *Aquatic Mammals*, 45(2):125–232.

Tetra Tech (2012). Block Island Wind Farm and Block Island Transmission System Environmental Report / Construction and Operations Plan. Technical report, Submitted by Deepwater Wind, Boston, MA.

Tetra Tech and JASCO (2015). Hydroacoustic Monitoring Program Final Technical Report Block Island Wind Farm Construction 2015. Technical report, Prepared for Deepwater Wind Block Island, LLC.

Westwood, E. K., Tindle, C. T., and Chapman, N. R. (1996). A normal mode model for acousto-elastic ocean environments. *The Journal of the Acoustical Society of America*, 100(6):3631–3645.

Wilkes, D. R. and Gavrilov, A. N. (2017). Sound radiation from impact-driven raked piles. *Journal of the Acoustical Society of America*, 142(1):1–11.

Zampolli, M., Nijhof, M. J. J., de Jong, C. A. F., Ainslie, M. A., Jansen, E. H. W., and Quesson, B. A. J. (2013). Validation of finite element computations for the quantitative prediction of underwater noise from impact pile driving. *The Journal of the Acoustical Society of America*, 133(1):72–81.

MANUSCRIPT 3

Fin whale localization and environmental inversion using modal arrivals of the 20-Hz pulse

This manuscript is currently unpublished.

Jennifer L. Amaral, James H. Miller and Gopu R. Potty

Department of Ocean Engineering, University of Rhode Island, Narragansett, RI 02882, USA

Ying-Tsong Lin

Applied Ocean Physics and Engineering, Woods Hole Oceanographic Institution, Woods Hole, MA 02543, USA

Kathleen Vigness-Raposa

INSPIRE Environmental, 513 Broadway, Suite 314, Newport, RI 02840, USA

Abstract: Fin whale doublet calls, described as two 20-Hz pulses recorded at different interpulse intervals, have been attributed to the whale's calling behavior, however they could also result from acoustic mode propagation effects. Modes travel with their own frequency-dependent group velocities. The dispersion of these modes results in the sound being recorded as multiple arrivals on a receiver. Multiple modal arrivals of 20-Hz fin whale calls were recorded, with mode one arriving after mode two. The time delay between modal arrivals varied throughout the recording and is range dependent. The range dependency of this time delay was used to estimate the range of the whale from individual hydrophones by determining the modal group velocities that resulted in the observed delays. A pair of hydrophones was used to localize the whale for the duration of time when two modes were detected. The KRAKEN normal mode model was utilized in an inversion scheme to determine the compressional wave speed and depth to bedrock in the study area that supported the estimated modal group velocities. The inversion resulted in a depth to bedrock of 205 m and compressional wave speed of 1735 m/s, which were supported by measurements reported in literature for nearby regions. [Work supported by BOEM]

3.1 Introduction

Fin whales (*Balaenoptera physalus*) produce stereotyped low frequency songs that are composed of a series of 20-Hz pulses that repeat at consistent time intervals for long durations and have been recorded worldwide (Širović et al., 2007; Rebull et al., 2006; Weirathmueller et al., 2017; Thompson et al., 1992; Castellote et al., 2012; Miksis-Olds et al., 2019). The 20-Hz pulse is a high-amplitude and short-duration chirp lasting less than 1 second that sweeps down in frequency between approximately 23 to 18 Hz (Watkins et al., 1987). A sequence of regularly occuring 20-Hz pulses is known as a song and a sequence of songs is known as a song bout (Clark et al., 2019). Individual fin whale songs within a bout are separated from each other by silent periods that occur at approximtely 15 minute intervals (Watkins et al., 1987). Within a song, consecutive 20-Hz pulses occur at consistent time intervals, which is referred to as the interpulse interval, and is the time between successive pulses measured from a point on one pulse to the same point on a succeeding pulse (Thompson et al., 1992).

The composition of recorded fin whale song has been described as 20-Hz pulses repeating at regularly repeated pulse intervals, either at one nominal pulse rate (singlet) or at two alternating pulse intervals (doublet) (Thompson et al., 1992; Watkins et al., 1987). This doublet phenomenon has been attributed to the fin whale's calling behavior, but additional observations have been made that suggest the 20-Hz doublet pattern could be explained by multipath arrivals of a single 20-Hz pulse at the acoustic instrument rather than the fin whale emitting two pulses at alternating interpulse intervals (Premus and Spiesberger, 1997). If the doublet pattern is an artifact of propagation, then information contained within the recorded signal could be used for passive ranging and localization of the whale and geoacoustic inversions to estimate environmental parameters (Premus and

Spiesberger, 1997; Kuna and Nábělek, 2021).

Multipath propagation in shallow water environments can be described by normal mode theory. A normal mode is described as a standing wave between the boundaries of an acoustic waveguide that propagates horizontally with a frequency-dependent group speed (Jensen et al., 2011). The number of propagating modes depends on the depth of the waveguide and frequency of the source. As a pulse propagates down a waveguide, the individual modes will travel at independent group velocities and arrive at a receiver at different times, known as modal dispersion.

In shallow water waveguides, recorded calls from whales at ranges of more than several water depths may become distorted due to multimode dispersion (Wiggins et al., 2004; Lin et al., 2012). Premus and Spiesberger (1997) discussed that the time delay between modal arrivals is strongly range dependent and can be used, in conjunction with geoacoustic knowledge of the environment, to estimate the range of the whale using only a single hydrophone. Additionally, passive localization can be achieved using only a pair of hydrophones. While the range estimate is insensitive to the depth of the whale, the ranging can only be achieved when multiple modes are detected. Detection of these modes is limited by the detection range of the first arrival which is typically the water-borne pulse, but also could be the sediment-refracted/basement-reflected path if the compressional wave speed in the sediment layers is higher than that in the water column (Premus and Spiesberger, 1997).

The study presented in this paper focuses on the use of multipath arrivals of 20-Hz fin whale calls to localize a whale and invert for environmental properties in a shallow water study area. Multiple arrays were deployed off the coast of Block Island, Rhode Island, USA that recorded a fin whale of opportunity as it

vocalized for over eighteen hours in the vicinity of the sensors. Individual 20-Hz pulses arrived at the receiver as two distinct modes and the time delay between modal arrivals varied throughout the recording. The range dependency of this time delay was exploited to estimate the range of the whale from individual sensors by determining the modal group velocities that resulted in the observed time delays. Once the range of the whale from individual hydrophones was found, a pair of hydrophones was used to localize the whale for the duration of time when two modes were detected in the recorded data. The KRAKEN normal mode model was then used to invert for the sediment compressional wave speed and depth to bedrock in the study area that supported the estimated modal group speeds.

The paper is organized in the following manner. Section II describes the study location along with the measurement equipment. Section III presents the method used to detect the fin whale calls in the dataset. Sections IV and V present the fin whale and modal detections. Secton VI presents the method used to determine the range difference of the whale from the deployed arrays. Section VII presents the fin whale detections recorded on a different deployed sensor suite that was used to validate the detections on the deployed arrays. Section VIII dicusses the localization of the whale and Section VIIII presents the inversion method and results. A discussion is presented in Section X, followed by the conclusions of the study in Section XI.

3.2 Measurement Equipment

Two vertical line arrays (referred to as Array 1 and Array 2) were deployed for 24 days between October and November 2015 off the coast of Block Island, Rhode Island, USA (Figure 3.1). These sensor systems were deployed as part of the Bureau of Ocean Energy Management (BOEM) funded Real-time Opportunity for Development Environmental Observations (RODEO) program with the objec-

tive of recording the underwater sound generated during impact pile driving to install the Block Island Wind Farm (BIWF) turbine foundations. Fin whale 20-Hz vocalizations were recorded as sources of opportunity during the deployment of the arrays.

Each vertical line array consisted of four HTI-94-SSQ model hydrophones from High Tech, Inc. with a sensitivity of -170 dB re 1V/μPa, where each hydrophone was spaced 5 m apart and located at water depths from 20 to 35 m. All sensors were continuously recording on Several Hydrophone Receive Units (SHRUs) at a rate of 9765.62 Hz for the duration of deployment. The arrays were deployed in approximately 40 m of water with an inter-array spacing of 7.5 km.

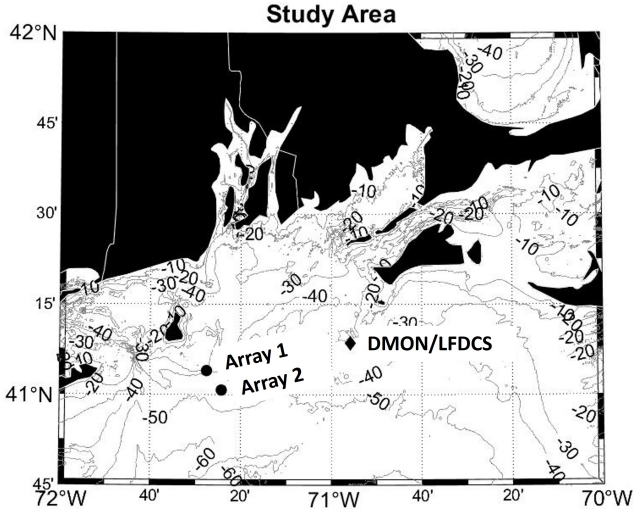

Figure 3.1. Location of the vertical line arrays (Array 1 and Array 2) deployed off the coast of Block, Island, Rhode Island, USA during October and November 2015. A DMON/LFDCS system deployed by Woods Hole Oceanographic Institution during this time as part of a separate effort was located 42-45 km east of Array 1 and Array 2 (Baumgartner and Lin, 2019). Depth contours are in meters.

3.3 Analysis Method

A long duration bout of 20-Hz pulses was detected on all of the hydrophones in the two vertical arrays. Custom scripts were developed in MATLAB R2019a

(www.mathworks.com) to detect and analyze the recorded 20-Hz pulses for the entire duration of the recording. The acoustic recordings were decimated to a sampling rate of approximately 1 kHz to allow for more efficient processing and analysis. Data were then band pass filtered (fifth-order Chebyshev type II) between 10-30 Hz prior to detecting the pulses. The data from a single sensor on either array were utilized for the analysis presented in this paper. The sensors located at a depth of 25 m on Array 1 and at a depth of 26 m on Array 2 were used for further analysis because they had the highest received levels on each array. A segment of data showing three individual songs within the recorded bout is shown in Figure 3.2.

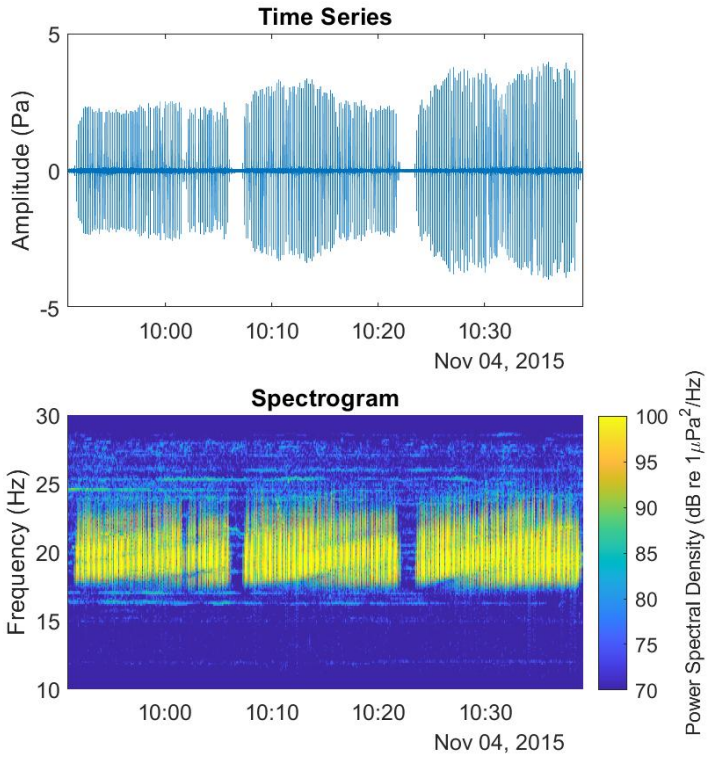

Figure 3.2. Time series (top) and spectrogram (bottom) of a segment of the fin whale bout recorded on a single hydrophone in Array 2 (hydrophone at 26 m depth) showing three individual songs. Data has been bandpass filtered to improve SNR of the 20-Hz pulses. Time axis is UTC.

3.4 Modal Detections

Two distinct modal arrivals of individual 20-Hz pulses were observed in the data recorded on the arrays (Figure 3.3) and scripts were written to detect and analyze each modal arrival separately. Higher mode numbers traditionally correspond to higher grazing angles and therefore higher modes would penetrate deeper into seafloor at the frequencies of interest to this paper. If the compressional wave speed in the sediment is higher than the sound speed through the water column then the sediment-refracted/basement-reflected path could arrive first. The waveguide in this study area is thought to encompass the sediment/subfloor layers in addition to the water column and the compressional wave speed in the sediment is higher than that in the water column, therefore the sediment-dominated mode is estimated to arrive first.

The mode one arrival of the 20-Hz pulse was detected by cross correlating the time series with a representative 20-Hz pulse. The representative pulse used was selected from the data as a pulse that had a high signal-to-noise ratio and only one modal arrival. Correlations above a threshold were classified as detections and saved for further analysis. All detections were manually verified and false detections were disregarded.

The mode two arrival was lower in both amplitude and bandwidth than the mode one arrival and arrived before the mode one arrival (Figure 3.3). The mode two arrivals were detected by finding peaks in the envelope of the time series signal above a threshold that arrived before the largest amplitude detection. All detections were manually verified and false detections were disregarded. The lower amplitude modal arrivals that had a peak-signal to rms-noise ratio above 15 dB were included in further analysis.

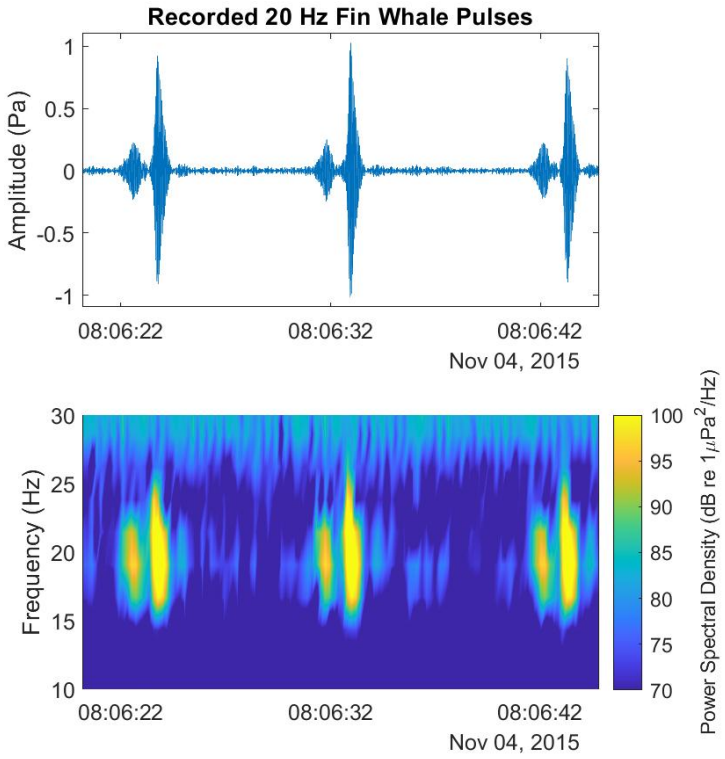

Figure 3.3. Time series (top) and spectrogram (bottom) showing three fin whale 20-Hz pulses recorded on a single hydrophone in Array 1. Two distinct and time separated arrivals are clearly seen in both the time series and spectrogram representation. The interpulse interval between the larger amplitude arrivals (mode one) is approximately 10 seconds. The receiver was at 25 meters depth. Time axis is UTC.

3.5 Detections

The 20-Hz pulses were detected in the recordings from both arrays for over eighteen hours. The received sound pressure level recorded during the fin whale bout was generally higher on Array 2 as compared to Array 1. The maximum received level of the mode one arrival on Array 1 was 129 dB re 1μPa (peak) and was 143 dB re 1μPa (peak) on Array 2. The higher received levels recorded on Array 2 suggest that the whale traveled closer to this array than Array 1 (Figure 3.4 (top)).

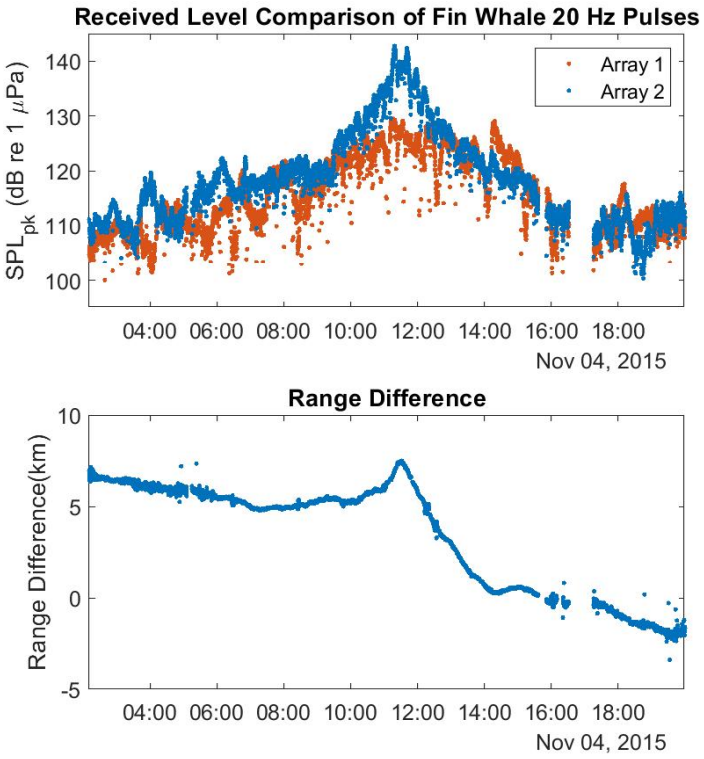

Figure 3.4. Comparison of the peak sound pressure levels (dB re 1μPa) from the larger amplitude modal arrival measured on both arrays throughout the recorded bout (top). Difference in the path length of the fin whale signals received on a single sensor in both arrays. A positive distance means the signal was received on Array 2 before Array 1 and a negative distance means the signal was received on Array 1 before Array 2 (bottom). The hydrophone used to generate these data is at a depth of 25 m on Array 1 and 26 m on Array 2. Time axis is UTC.

Long duration 20-Hz song bouts are thought to be breeding displays made by male fin whales (Croll et al., 2002). The evidence supports the hypothesis that these vocalizations were from one male fin whale because the bout was recorded at the beginning of the reproductive season, which runs from November through May (Morano et al., 2012), and there were no overlapping detections throughout this song bout. Watkins (1981) also observed that these patterns of 20-Hz pulses were mostly heard in the winter season and were produced by only one fin whale either traveling in a group or separated from other fin whales by several kilometers.

Sequential pulses within a bout are relatively constant in level, but the pulses immediately following or preceding a quiet period have been found to be of lower level in recordings made in both the Atlantic (Watkins et al., 1987) and North Pacific (Helble et al., 2020). This phenomenon was also observed in the recorded signal bout. No explanation has been provided for these lower levels, but it has been theorized that they could be due to lower source levels from the fin whale or due to higher acoustic transmission loss when the whale is closer to the surface (Helble et al., 2020), assuming the whale is surfacing during the rest periods.

3.6 Range Difference

The difference in arrival time of mode one on a single sensor in each array was measured. This difference in arrival time was used to calculate the range difference of the whale between the arrays (Figure 3.4 (bottom)). The maximum difference in range is 7.5 km, which is the spacing between the two arrays. This maximum difference in range would be expected when the whale's position was directly in line with the two arrays, which would imply the signal arrived on Array 2 first and then traveled 7.5 km before reaching Array 1.

The received levels recorded on Array 2 were higher than those recorded on Array 1 up through approximately 13:00, before the received levels became similar on both arrays (Figure 3.4 (top)). This implies that the whale was closer to Array 2 up until this time and then the whale traversed a track that was a similar distance from both arrays. This is confirmed by the variation in the range difference. As the whale approaches the arrays, it is farther from Array 1 than it is from Array 2. The range difference between arrivals is maximum at 11:30, which coincides with the time of the maximum received sound levels measured on Array 2. This is the time of the closest point of approach of the whale to the arrays. As the whale moves away from the arrays, it follows a path bringing it closer to Array 1. After

16:00 it is traveling a path that is closer to Array 1 than Array 2.

3.7 Verification of Detections

A moored buoy system designed to detect, classify, and report the sounds of large whales in near-real-time that was part of a separate study (Baumgartner and Lin, 2019) was deployed near Martha's Vineyard, Massachusetts, USA during the same time that the arrays in this study were deployed. The buoy was 45 km east of Array 1 and 42 km east of Array 2 (Figure 3.1) in a water depth of 34 m and was equipped with a digital acoustic monitoring (DMON) instrument that was running a low frequency detection and classification system (LFDCS). The DMON/LFDCS detects and classifies tonal sounds of baleen whales in near real time and sends the detection data shore-side to be reviewed. The number of species specific detections in a 15-minute period within the acoustic detection range of the buoy were made available to the public after they had been verified.

The DMON/LFDCS automatically detects and classifies fin whales based on the 20-Hz pulse. Fin whales detected by the DMON/LFDCS had the lowest missed detection rate compared to other species and had a near-real-time false detection rate of nearly 0 percent. The DMON/LFCDS system was not used for localization, but the fin-whale specific acoustic detection range of the system was estimated at 30-40 km (Baumgartner and Lin, 2019). This estimate was based on acoustic detections and visual sightings at 40 km spatial scales and 24-72 hr temporal scales. It is possible that the detection range is less or more than this spatial scale since the acoustic and visual detections were not simultaneous, although this detection range was consistent with the 30 km detection range determined by Cholewiak et al. (2018) in a similar shallow environment of Massachusetts Bay.

The detection record of fin whales on November 4, 2015 showed that the DMON/LFDCS detected the largest number of fin whale 20-Hz pulses about 6

hours and 45 minutes before the highest sound levels were measured on the arrays (Figure 3.5). It is assumed that the pulses recorded on the arrays were made by a single fin whale and that the DMON detections were of that same whale. Examples of DMON recorded data show a single fin whale 20-Hz pulse that repeated at regular intervals of approximately every 10 seconds (pitch track (PT) data for 11/03/15 23:19:32 EST available on http://dcs.whoi.edu/nomans0315/nomans0315.shtml), which was similar to what was recorded on the arrays. From the time series of DMON/LFDCS detections it was inferred that the fin whale traveled through the detection range of the system toward the array locations and was beyond the detection range of the DMON at the time of the highest measured sound levels on the arrays. Since the arrays were able to detect the fin whale calls during the earlier times, it is assumed that the detection range of the arrays is farther than the 40 km DMON detection range.

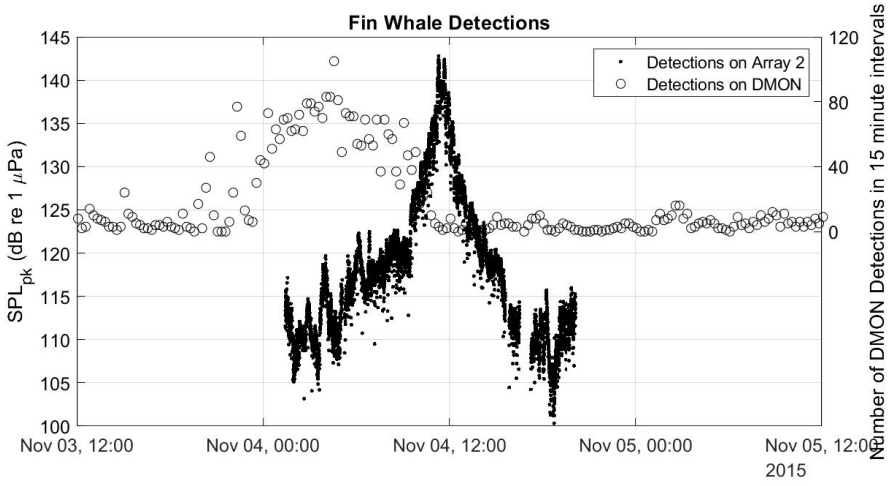

Figure 3.5. Comparison of the peak sound pressure levels (dB re 1μPa (peak)) recorded on Array 2 and the number of fin whale detections on the DMON buoy on November 4, 2015. Time axis is UTC.

3.8 Localization Using Modal Arrivals

In normal mode theory, a signal measured on a receiver will be the summation of all of the modes, however, individual modes traveling at different group velocities will arrival at different times. The group velocity of a mode is the velocity at which energy in the mode is transported. The number of propagating modes in a wave guide is dependent on frequency and no sound can propagate at frequencies below the cutoff frequency for the first mode, which is dependent on the depth of the water, the sound speed in water, and the sound speed in the sediment (Urick, 1983).

Two distinct modal arrivals of the 20-Hz pulse were seen in the data collected on the arrays. Multiple modes were not detectable prior to 07:00 or later than 15:30 in the dataset because the signal-to-noise ratio (SNR) of the higher order modes was not greater then the ambient noise levels. The amplitude of mode one was higher than the amplitude of mode two in the recorded data (Figure 3.6).

The time delay between the arrivals in the mode pairs from Figure 3.6 was calculated. The time delay data was smoothed by taking the average time delay in each song. The median song duration was 14 minutes long, so the average time delay was taken every 14 minutes.

The time difference between the modal arrivals on a single hydrophone varied throughout the recording (Figure 3.7) and was a function of the range of the whale from the sensor. The time difference between arrivals was greater earlier in the recording and decreased as the whale approached the array. Only one arrival was identifiable in the data from Array 2 when the whale was closest to Array 2, although two arrivals were seen in the data from Array 1 during this same time.

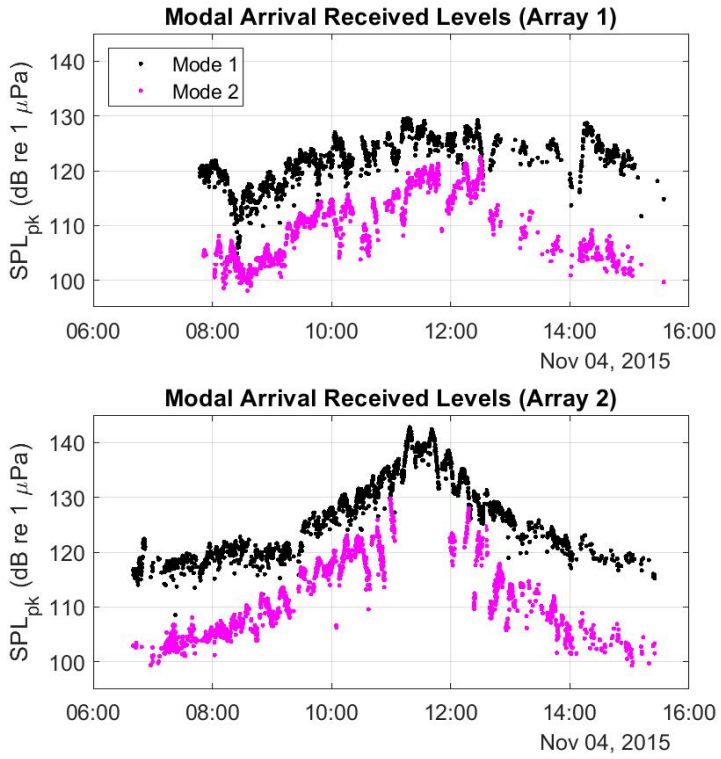

Figure 3.6. Peak sound pressure levels (dB re 1μPa (peak)) of the individual modal arrivals on a single sensor in each array. The sensor was at a depth of 25 m in Array 1 and 26 m in Array 2. Time axis is UTC.

3.8.1 Range Estimate

The range of the whale from each array was calculated using Equation 3.1, where R is the range of the whale in meters, v is the group speed of the indicated modal arrival, and Δt is the difference in arrival time between the two modes as measured in the received signal of a single sensor. The modal group speeds are unknown, but the measured range difference (Figure 3.4 (bottom)) was used to limit the range estimate. The measured modal time delays from Figure 3.7 and estimates of the modal group speeds were used to calculate the distance of the whale from each array. The range of the whale from both arrays was estimated assuming group speeds between 1400 and 1800 m/s. The root-mean-square error of

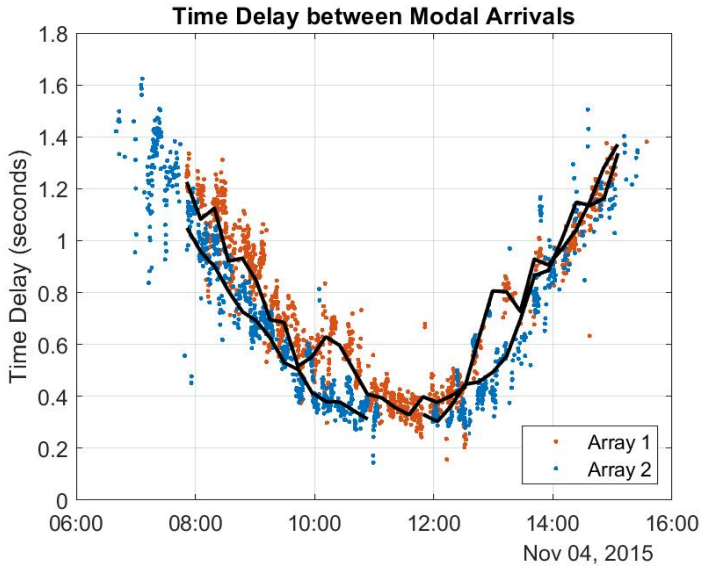

Figure 3.7. Time delay (in seconds) between the mode two and mode one arrivals in the records of both arrays when two modes could be resolved in the received time series. The average time delay in 14-minute time intervals (representing indidivudal songs) was calculated to smooth the data. Black lines are the average modal time delays for the individual songs in the bout. These average time delays were used to determine the range of the whale from the arrays. Time axis is UTC.

the difference in the range estimate from Array 2 and Array 1 was determined. The combination of modal group speeds that resulted in the smallest root-mean-square error were considered the optimal group speeds.

$$R = \frac{v_2 v_1 \Delta t}{v_2 - v_1} \tag{3.1}$$

The range of the whale from both arrays (Figure 3.8) was calculated using Equation 3.1 with these optimal modal group speeds(v_1, v_2) and the measured modal time delays (Δt). Since two distinct modal arrivals were not distinguishable on Array 2 during the closest point of approach, the range of the whale from Array 2 during this time was not able to be resolved using the modal time delay. However the difference in signal path length between the two arrays was used to determine the whale range during this time frame. The estimated range of the whale from

Array 1 was adjusted by the range difference to yield an estimate of the whale range from Array 2 (Figure 3.8 (black line)). The range estimated using both methods was similar during the whale approach and departure, but the estimate using the range difference was able to resolve the closest point of approach of the whale from Array 2.

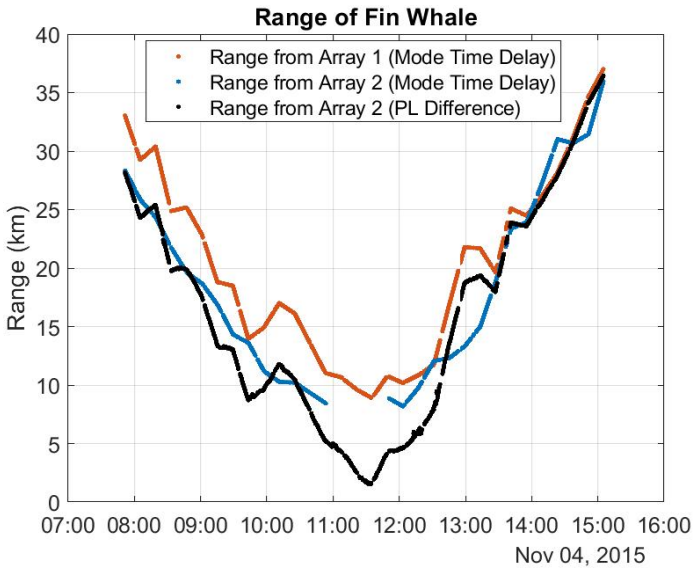

Figure 3.8. Estimated range of the whale from each array that was calculated assuming a group speed of 1563 m/s for mode one and a group speed of 1659 m/s for mode 2 (blue and orange lines). The whale's range from Array 2 when it was closest could not be resolved using the time difference between modes, so the range was estimated using the difference in range (black line). The two methods of calculating the whale range from Array 2 compare well during the approach and departure of the whale. Time axis is UTC.

3.8.2 Localization

The estimate of the whale's range from the pair of sensors (one from each array) was used to determine the whale's track. At each time step, a circle centered on each sensor with a radius equal to the range of the whale from that sensor was drawn. The intersection of the two range circles was a potential location of the whale. There were two intersection points for each time step, which yielded two

potential whale tracks. Since the fin pulses were detected on the DMON buoy before the arrays, the whale was assumed to be traveling from the northeast, so tracks that showed the whale traveling from the southwest were disregarded. Also a large number of fin whale calls were not detected on the DNOM after 12:00 (Figure 3.5) and it is unlikely that this whale turned around to travel back towards the DNOM location at any point during the track. This is supported by observations of fin whale singers that have been tracked swimming with fairfly consistent directions of travel (Clark et al., 2019). Therefore, the localization that produced a track with the fin whale traveling from northeast to southwest was determined to be the most plausible track (Figure 3.9).

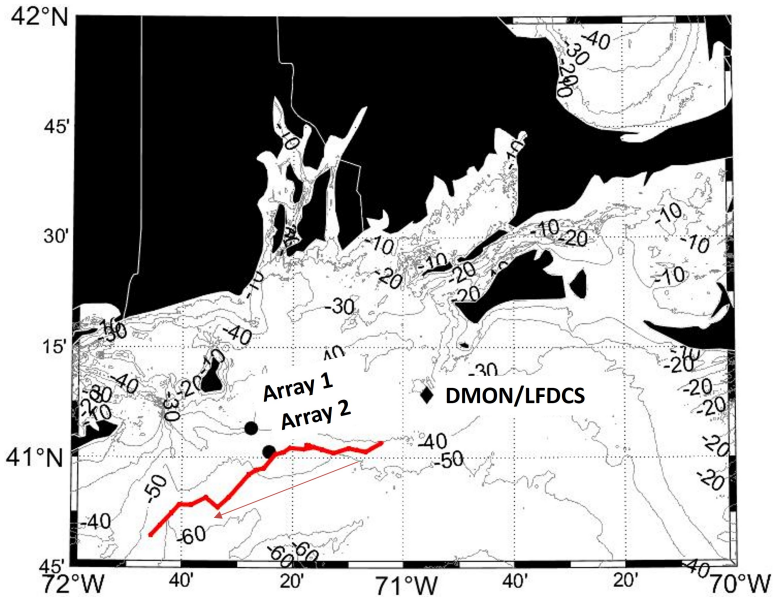

Figure 3.9. Most plausible path that the fin whale traveled on November 4, 2015 between 07:00 and 15:30 past the locations of the deployed arrays. Arrow indicates the direction of travel from northeast to southwest.

3.9 Inversion for Environmental Properties

The number of modes excited in a waveguide and the group speed of these modes are sensitive to environmental parameters such as the water depth, sediment

layer depth, and the sound speed through water and the sediment. The environmental properties of the study area are not known with a high degree of certainty, but can be inverted for using the modal group speed estimates used to determine the whale's range. The observations of two modal arrivals in the recorded data and a faster propagating mode two are important since the environmental parameters must support this type of propagation.

In this study the mode functions for the shallow water environment where the arrays were deployed were calculated by using the KRAKEN normal mode program (Porter, 1991). The estimated track shows the fin whale traveling in water depths of approximately 50 meters, thus a water depth of 50 m with an isovelocity sound speed profile of 1500 m/s were assumed. Fin whales typically vocalize while swimming at depths between 10-20 m (Kuna and Nábělek, 2021) therefore the source was input at a depth of 15 m representing a fin whale vocalizing at 20-Hz. A layered environment was assumed with 50 m of water overlaying a sediment layer of unknown depth that extends down to bedrock. The bedrock was modeled with a compressional sound speed of 3000 m/s and a density of 2.4 g/cc (Jensen et al., 2011).

KRAKEN was run assuming different combinations of sediment layer depth and sediment compressional sound speed. The difference between the modeled modal group speeds and the estimated modal group speeds (v_1 = 1593 m/s, v_2 = 1659 m/s) was determined and the combination of sediment sound speed and depth to bedrock input into the model that resulted in the smallest group speed differences were the most likely environmental parameters. The inversion scheme predicted a depth to bedrock of 205 meters and a sediment sound speed of 1735 m/s.

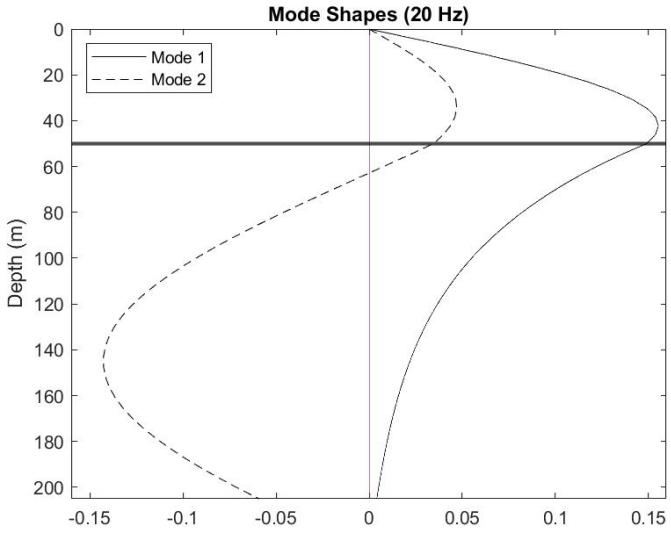

Figure 3.10. Depth dependence of the normal modes estimated using KRAKEN assuming a water depth of 50 m (bold line), sound speed in the water of 1500 m/s, sound speed in the sediment of 1735 m/s, a depth to bedrock of 205 m, and a sound speed in the bedrock of 3000 m/s. Two modes are supported in this environment, with the group speed of mode two being faster than that of mode one.

3.10 Discussion

The estimated track of the fin whale showed it travel a distance of 73.5 km at an average speed of 10.2 km/hr, with a maximum estimated detection range of over 30 km from the sensors. If the fin whale was following a fairly constant path as it approached and departed from the arrays, then the fin whale calls were detected at farther ranges than 30 km, but were unable to be localized using this method because two modal arrvials were not detected. The mode one arrival was detected at earlier and later times in the data, but the mode two arrival was not detectable due to low SNR at these same times. Baumgartner and Lin (2019) visually confirmed acoustic detections of fin whales within 40 km of the DMON system, although the acoustic and visual detections were not simultaneous so the whale's precise location at the time of vocalization was not known.

The range at which the calls can be detected by acoustic instruments is largely

influenced by environmental conditions. Fin whale 20-Hz pulses have been acoustically detected in shallow water environments at ranges of 30 km (Cholewiak et al., 2018) and in deep water environments at ranges of 56 km (Širović et al., 2007). The detection range is also sensitive to the local ambient noise levels. Modeled detection ranges varied between less than 10 km assuming higher ambient noise conditions out to 100 km at lower ambient noise levels (Stafford et al., 2007).

Previous studies of the bottom sediment types performed in the area of Block Island, Rhode Island have identified surficial sediment as sand and gravel. Grab samples and underwater video taken near the Block Island Wind Farm turbine locations confirmed a seabed dominated by medium and coarse sand, gravel and cobble sediments (HDR, 2018). Borings taken near the same site characterized the upper 70 meters of the seafloor and showed a surficial layer of sand and gravel that overlays layers of sand, clay, and silt (Sheldon, 2012). The estimated sediment sound speed of 1735 m/s is representative of a sandy environment that has been observed in this area as described in the studies mentioned. Additionally, a modeling study performed by Lin et al. (2019) used a sediment sound speed of 1725 m/s for this same study area, which is consistent with the speed of 1735 m/s estimated in this study. The estimate of 1725 m/s was extracted from the Deck41 seafloor surficial sediment database (Bershad and Weiss, 1976).

Verifying the depth to bedrock is more difficult as few measurements exist. The available data discuss a depth to bedrock consistent with the estimated depth of 205 meters. Seismic surveys in this area showed potential bedrock at a depth of up to and greater than 180 meters below the sea surface (Sheldon, 2012; Needell et al., 1983).

The current inversion scheme assumes that the water depth, sound speed in the water, and sediment layer depth is constant over the track of the fin whale.

It also assumes that there is a layer of water overlying a single sediment layer above a basement layer. In reality, the water depth, sound speed, and sediment layer depth might actually be varying over the fin whale track and there could be multiple sediment layers with different sound speeds. This variation is not currently captured in the inversion scheme because it is unknown. Assumptions can be made to include more detail in the inversion scheme, but the current scheme produces an average of the environmental parameters over the fin whale track. To add more detail, the inversion could be run assuming different water depths since the estimated fin whale track has the whale traveling through various depths. The inversion scheme could be broken up into different segments based on the water depth to invert for the varying environmental parameters in these different depth bins if necessary, but the average values along the track might be enough for specific applications.

3.11 Conclusion

A fin whale was recorded vocalizing for over eighteen hours on two vertical line arrays that were deployed off the coast of Block Island, Rhode Island, USA. The signal received on the arrays arrived as two distinct modes, with mode two arriving before mode one due to the higher group velocity of the second mode. The 20-Hz pulses observed in this dataset were a single call that arrived as two arrivals due to modal dispersion and support the hypothesis that the fin whale doublet calls could be mulitpath arrivals and not produced as a doublet by the whale. The time delay between the modal arrivals on a single hydrophone and the time difference in arrival between the mode one arrival on a pair of hydrophones were used to determine the most likely range and track of the whale from the sensors. Fin whale detections recorded during the same time period on a separate deployed system were used to validate the estimated whale track. The modal group speeds

and range estimate of the whale were used to invert for the environmental parameters of the study area, which resulted in an estimate of the depth to bedrock and sediment compressional sound speed that were consistent with previous measurements. This paper presents a method of using modal arrivals of fin whale 20-Hz pulses to estimate a whale's range using a single sensor and the whale's location using a pair of sensors. The analysis could be extended further to invert for the average environmental parameters along the whale's track that support the observed acoustic propagation.

Acknowledgments: The data used for this research was collected as part of the U.S. Department of the Interior, Bureau of Ocean Energy Management (BOEM), Environmental Studies Program, Washington, DC under Contract Number M15PC00002, Task Order M16PD00025. Collaborators in this project include Randy Gallien and Anwar Khan (HDR, Inc.).

Bibliography

Baumgartner, M. F. and Lin, Y.-T. (2019). Evaluating the Accuracy and Detection Range of a Moored Whale Detection Buoy near the Massachusetts Wind Energy Area. Technical report, Woods Hole (MA): Massachusetts Clean Energy Center and U.S. Department of the Interior, Bureau of Ocean Energy Management.OCS Study BOEM 2019-061.

Bershad, S. and Weiss, M. (1976). Deck41 Surficial Seafloor Sediment Description Database. NOAA National Centers for Environmental Information. https://doi.org/10.7289/V5VD6WCZ.

Castellote, M., Clark, C. W., and Lammers, M. O. (2012). Fin whale (Balaenoptera physalus) population identity in the western Mediterranean Sea. *Marine Mammal Science*, 38:325–344.

Cholewiak, D., Clark, C. W., Ponirakis, D., Frankel, A. S., Hatch, L. T., Risch, D., Stanistreet, J. E., Thompson, M., Vu, E., and Van Parijs, S. M. (2018). Communicating amidst the noise: modeling the aggregate influence of ambient and vessel noise on baleen whale communication space in a national marine sanctuary. *Endangered Species Research*, 36:59–75.

Clark, C. W., Gagnon, G. J., and Frankel, A. S. (2019). Fin whale singing decreases with increased swimming speed. *Royal Society Open Science*, 6.

Croll, D. A., Clark, C. W., Acevedo, A., Tershy, B., Flores, S., Gedamke, J., and Urban, J. (2002). Only male fin whales sing loud songs. *Nature*, 417:809.

Cummings, W. C., Thompson, P. O., and Ha, S. J. (1986). Sounds from Bryde,

Balaenoptera edeni, and finback, B. physalus, whales in the Gulf of California. *Fishery Bulletin*, 84(2):359–370.

Rebull, O. G., Cusí, J. D., Ruiz Fernández, M., and Muset, J. G. (2006). Tracking fin whale calls offshore the Galicia Margin, North East Atlantic Ocean. *The Journal of the Acoustical Society of America*, 120(4):2077–2085.

HDR (2018). Benthic Monitoring During Wind Turbine Installation and Operation at the Block Island Wind Farm , Rhode Island. Technical report, Final Report to the U.S. Department of the Interior, Bureau of Ocean Energy Management, Office of Renewable Energy Programs.

Helble, T. A., Guazzo, R. A., Alongi, G. C., Martin, C. R., Martin, S. W., and Henderson, E. E. (2020). Fin Whale Song Patterns Shift Over Time in the Central North Pacific. *Frontiers in Marine Science*, 7.

Jensen, F. B., Kuperman, W. A., Porter, M. B., and Schmidt, H. (2011). *Computational Ocean Acoustics*. Springer Science, New York, NY, second edition.

Kuna, V. M. and Nábělek, J. L. (2021). Seismic crustal imaging using fin whale songs. *Science*, 371:731–735.

Lin, Y.-T., Newhall, A. E., and Lynch, J. F. (2012). Low-frequency broadband sound source localization using an adaptive normal mode back-propagation approach in a shallow-water ocean. *The Journal of the Acoustical Society of America*, 131(2):1798–1813.

Lin, Y.-T., Newhall, A. E., Miller, J. H., Potty, G. R., and Vigness-Raposa, K. J. (2019). A three-dimensional underwater sound propagation model for offshore wind farm noise prediction. *The Journal of the Acoustical Society of America*, 145(5):EL335–EL340.

Miksis-Olds, J. L., Harris, D. V., and Heaney, K. D. (2019). Comparison of estimated 20-Hz pulse fin whale source levels from the tropical Pacific and Eastern North Atlantic Oceans to other recorded populations. *Journal of the Acoustical Society of America*, 146(4):2373–2384.

Morano, J. L., Salisbury, D. P., Rice, A. N., Conklin, K. L., Falk, K. L., and Clark, C. W. (2012). Seasonal and geographical patterns of fin whale song in the western North Atlantic Ocean. *The Journal of the Acoustical Society of America*, 132(2):1207–1212.

Needell, S. W., O'Hara, C. J., and Knebel, H. J. (1983). Maps showing geology and shallow structure of western Rhode Island Sound: U.S. Geological Survey Miscellaneous Field Studies Map MF-1537. Technical report, U.S. Geological Survey.

Nieukirk, S. L., Mellinger, D. K., Moore, S. E., Klinck, K., Dziak, R. P., and Goslin, J. (2012). Sounds from airguns and fin whales recorded in the mid-Atlantic Ocean , 1999-2009. *The Journal of the Acoustical Society of America*, 131(2):1102–1112.

Porter, M. B. (1991). The KRAKEN Normal Mode Program. Technical report, SACLANT Underwater Research Centre, La Spezia, Italy.

Premus, V. and Spiesberger, J. L. (1997). Can acoustic multipath explain finback (B. physalus) 20-Hz doublets in shallow water? *The Journal of the Acoustical Society of America*, 101:1127–1138.

Sheldon, D. P. H. (2012). *Stratigraphy of a Proposed Wind Farm Site Southeast of Block Island: Utilization of Borehole Samples, Downhole Logging, and Seismic Profiles*. PhD thesis, University of Rhode Island.

Širović, A., Hildebrand, J. A., and Wiggins, S. M. (2007). Blue and fin whale call source levels and propagation range in the Southern Ocean Blue and fin whale call source levels and propagation range in the Southern Ocean. *The Journal of the Acoustical Society of America*, 122(2):1208–1215.

Soule, D. C. and Wilcock, W. S. D. (2013). Fin whale tracks recorded by a seismic network on the Juan de Fuca Ridge, Northeast Pacific Ocean. *The Journal of the Acoustical Society of America*, 133(3):1751–1761.

Stafford, K. M., Mellinger, D. K., Moore, S. E., and Fox, C. G. (2007). Seasonal variability and detection range modeling of baleen whale calls in the Gulf of Alaska, 1999â€“2002. *The Journal of the Acoustical Society of America*, 122(6):3378–3390.

Thompson, P. O., Findley, L. T., and Vidal, O. (1992). 20-Hz pulses and other vocalizations of fin whales, Balaenopteraphysalus, in the Gulf of California, Mexico. *The Journal of the Acoustical Society of America*, 92(6):3051–3057.

Urick, R. J. (1983). *Principles of Underwater Sound*. Peninsula Publishing, Los Altos, CA, 3rd edition.

Watkins, W. A. (1981). Activities and Underwater Sounds of Fin Whales. *Sci. Rep. Whales Res. Inst*, 33:83–117.

Watkins, W. A., Tyack, P., Moore, K. E., and Bird, J. E. (1987). The 20-Hz signals of finback whales (Balaenoptera physalus). *The Journal of the Acoustical Society of America*, 82(6):1901–1912.

Weirathmueller, M. J., Stafford, K. M., Wilcock, W. S. D., Hilmo, R. S., Dziak, R. P., and Trehu, A. M. (2017). Spatial and temporal trends in fin whale

vocalizations recorded in the NE Pacific Ocean between 2003-2013. *PLOS One*, 12(10).

Wiggins, S. M., McDonald, M. A., Munger, L. M., Moore, S. E., and Hildebrand, J. A. (2004). Wavegu ide Propagation allows for Range Estimates for North Pacific Right Whales in the Bering Sea. *Canadian Acoustics*, 32(2):146–154.

MANUSCRIPT 4

Analysis and localization of fin whale 20-Hz pulses

This manuscript is currently unpublished.

Jennifer L. Amaral, James H. Miller and Gopu R. Potty

Department of Ocean Engineering, University of Rhode Island, Narragansett, RI 02882, USA

Ying-Tsong Lin

Applied Ocean Physics and Engineering, Woods Hole Oceanographic Institution, Woods Hole, MA 02543, USA

Kathleen Vigness-Raposa

INSPIRE Environmental, 513 Broadway, Suite 314, Newport, RI 02840, USA

Abstract: The 20-Hz pulse, a common fin whale vocalization, was recorded near continuously for an extended duration off the coast of Block Island, Rhode Island USA. This fin whale bout was recorded for over eighteen hours as a source of opporunity during the deployment of multiple sensors in a shallow water environment. Characteristics of the recorded vocalizations, including the received level, interpulse interval, and duration of the songs and rest periods were analyzed. The properties of the recorded song were consistent with those previously reported in literature. The analysis of the vocalizations revealed that the 20-Hz pulses arrived at the receivers as multiple modes, where the time delay between modal arrivals varied with the range of the whale from the receiver. The time delay between arrivals on spatially separated sensors and the time delay between the modal arrivals on a single sensor were used to localize and track the whale for a duration of 7.2 hours as it swam approximately 73 km past the deployed instruments. [Work supported by the BOEM]

4.1 Introduction

Fin whales (*Balaenoptera physalus*) produce stereotyped low frequency song bouts that have been recorded worldwide (Širović et al., 2007; Rebull et al., 2006; Weirathmueller et al., 2017; Thompson et al., 1992; Castellote et al., 2012; Miksis-Olds et al., 2019). These bouts consist of vocalizations known as 20-Hz pulses that are repeated at regular intervals to form songs that last for many hours (Watkins et al., 1987) and are thought to be breeding displays made by male fin whales (Croll et al., 2002). The 20-Hz pulse is a high-amplitude and short-duration chirp lasting less than 1 second that sweeps down in frequency between approximately 23 to 18 Hz (Watkins et al., 1987).

Within a song, consecutive 20-Hz pulses occur at consistent time intervals. This interval is referred to as the interpulse interval and is the time between successive pulses measured from a point on one pulse to the same point on a succeeding pulse (Thompson et al., 1992). The time interval has been known to vary seasonally (Morano et al., 2012) and can be used to explain a majority of the song variability between populations in the North Atlantic and North Pacific Oceans (Hatch and Clark 2004). The fundamental frequencies and intervals between the 20-Hz pulses are stable with distance and are thought to be the most important signal components to the whales (Watkins, 1981). A constant interpulse interval represents a single pulse pattern while a doublet pattern is represented by a pair of alternating short and long interpulse intervals (Watkins et al., 1987). The pattern can shift between doublet and single within a single recorded bout (Thompson et al., 1992).

The stereotyped characteristics and repetition of the 20-Hz pulses for long duration make the fin whale call well suited for detection, localization, and tracking. As fin whales are producing these long duration 20-Hz songs they have been observed in shallow dive routines (Watkins, 1981) with fairly consistent directions

of travel (Clark et al., 2019). The precise range at which fin whales may detect these signals from a vocalizing whale is not known (Nieukirk et al., 2012), but the low frequency vocalizations will travel over long distances. The range at which the calls can be detected by acoustic instruments is largely influenced by environmental conditions. Fin whale 20-Hz pulses have been acoustically detected in shallow water environments at ranges of 30 km (Cholewiak et al., 2018) and in deep water environments at ranges of 56 km (Širović et al., 2007). Baumgartner and Lin (2019) visually confirmed acoustic detections within 40 km of a deployed instrument, although the acoustic and visual detections were not simultaneous so the whale's precise location at the time of vocalization was not known. The detection range is also sensitive to the local ambient noise levels. Modeled detection ranges of instruments varied between less than 10 km assuming higher ambient noise conditions out to 100 km at lower ambient noise levels (Stafford et al., 2007).

For whales vocalizing within the detection range of acoustic instruments, the 20-Hz doublet pattern could be explained by multipath arrivals of a single 20-Hz pulse at the acoustic instrument rather than the fin whale emitting two pulses at alternating interpulse intervals (Premus and Spiesberger, 1997). Low frequency sounds traveling in shallow water experience dispersion of the acoustic normal modes. A normal mode is described as a standing wave between the boundaries of an acoustic waveguide that propagates horizontally with a frequency dependent speed (Jensen et al., 2011). A useful interpretation of an acoustic normal mode is the interference pattern of upward and downward propagating rays (Mikhalevsky, 2001). Higher mode numbers traditionally correspond to higher grazing angles. A higher mode (and its corresponding rays) therefore would penetrate deeper into seafloor at the frequencies of interest to this paper. In shallow water waveguides, calls received from whales at ranges of more than several water depths may become

distorted due to multimode dispersion (Wiggins et al., 2004). A pulse received on a hydrophone can therefore contain several modal arrivals that traveled at independent group velocities and arrived at different times. The time difference between the modal arrivals can be used to calculate the distance between source and receiver (Lin et al., 2012; Wiggins et al., 2004). Depending on the sound speed profile in the waveguide and the source frequency, the group velocity of mode 2 could be higher than mode 1 and arrive earlier (Frisk, 1994).

A single bout of 20-Hz fin whale pulses was recorded for an extended duration on various sensors deployed off the coast of Rhode Island, USA in shallow waters. The bout was recorded for a duration of eighteen hours, however it is likely that it lasted longer but was not recorded because the whale was beyond the detection range of the sensors. The sensors utilized in this study were not deployed for the purpose of marine mammal localization so the number and position of the sensors do not allow for typical localization methods to be used. Instead, the modal arrivals detected in the data on individual sensors were used to localize and track the whale as it moved past the deployed arrays. A single sensor from each array was used in the localization process. The characterisitcs of the recorded fin whale vocalizations as well as the estimated track of the whale will be presented in this paper.

The paper is organized in the following manner. Section II describes the study location along with the measurement equipment. Section III presents the method used to detect the fin whale calls in the dataset. Section IV discusses the analysis results including properties of the bout, received levels, and the range difference of the whale in relation to the deployed sensors. Section V presents the fin whale detections recorded on a different deployed sensor suite that was used to validate the detections on the deployed arrays. Section VI includes a discussion of

modal dispersion, how the recorded data were used to range and track the whale's location, and presents the results of the localization. Section VII discusses the main conclusions of this study.

4.2 Measurement Equipment

Two vertical line arrays (referred to as Array 1 and Array 2) were deployed for 24 days between October and November 2015 off the coast of Block Island, Rhode Island, USA (Figure 4.1). These sensor systems were deployed as part of the Bureau of Ocean Energy Management (BOEM) funded Real-time Opportunity for Development Environmental Observations (RODEO) program with the objective of recording the underwater sound generated during impact pile driving to install the Block Island Wind Farm (BIWF) turbine foundations. Fin whale 20-Hz vocalizations were recorded as sources of opportunity during the deployment of the arrays.

Each vertical line array consisted of four HTI-94-SSQ model hydrophones from High Tech, Inc. with a sensitivity of -170 dB re 1V/μPa, where each hydrophone was spaced 5 m apart and located at water depths from 20 to 35 m. All sensors were continuously recording on Several Hydrophone Receive Units (SHRUs) at a rate of approximately 10 kHz for the duration of deployment. The arrays were deployed in approximately 40 m of water with an inter-array spacing of 7.5 km.

4.3 Detection Method

A long duration bout of 20-Hz pulses was detected on all of the hydrophones in the two vertical arrays. Custom scripts were developed in MATLAB R2019a (www.mathworks.com) to detect and analyze the recorded 20-Hz pulses for the entire duration of the recording. The acoustic recordings were decimated to a sampling rate of approximately 1 kHz to allow for more efficient processing and

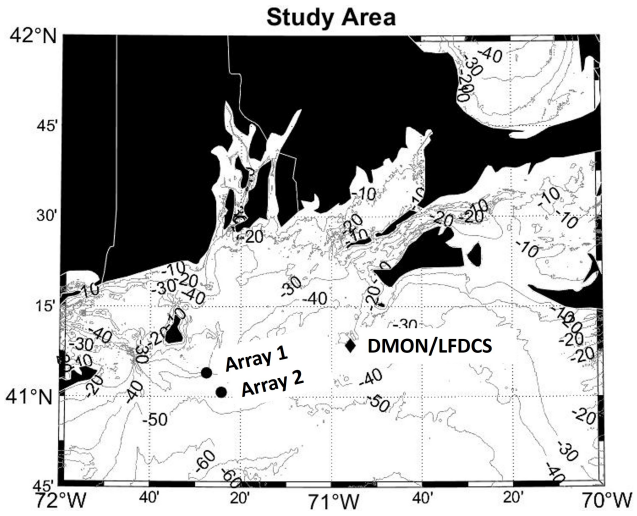

Figure 4.1. Location of the vertical line arrays (Array 1 and Array 2) deployed off the coast of Block, Island, Rhode Island, USA during October and November 2015. A DMON/LFDCS system deployed by Woods Hole Oceanographic Institution during this time as part of a separate effort was located 42-45 km east of Array 1 and Array 2 (Baumgartner and Lin, 2019). Depth contours are in meters.

analysis. Data were then band pass filtered (fifth-order Chebyshev type II) between 10-30 Hz prior to detecting the pulses. The data from a single sensor on either array were utilized for the analysis presented in this paper. The sensors located at a depth of 25 m on Array 1 and at a depth of 26 m on Array 2 were used for further analysis because they had the highest received levels on each array.

4.4 Recorded 20-Hz Pulses

A portion of the bout showing three distinct songs is shown in Figure 4.2. The recording supports the hypothesis that these vocalizations were from one male fin whale because the bout was recorded at the beginning of the reproductive season, which runs from November through May (Morano et al., 2012), and there were no overlapping detections throughout this song bout. Watkins (1981) also observed that these patterns of 20-Hz pulses were mostly heard in the winter season and were produced by only one fin whale either traveling in a group or separated from

other fin whales by several kilometers.

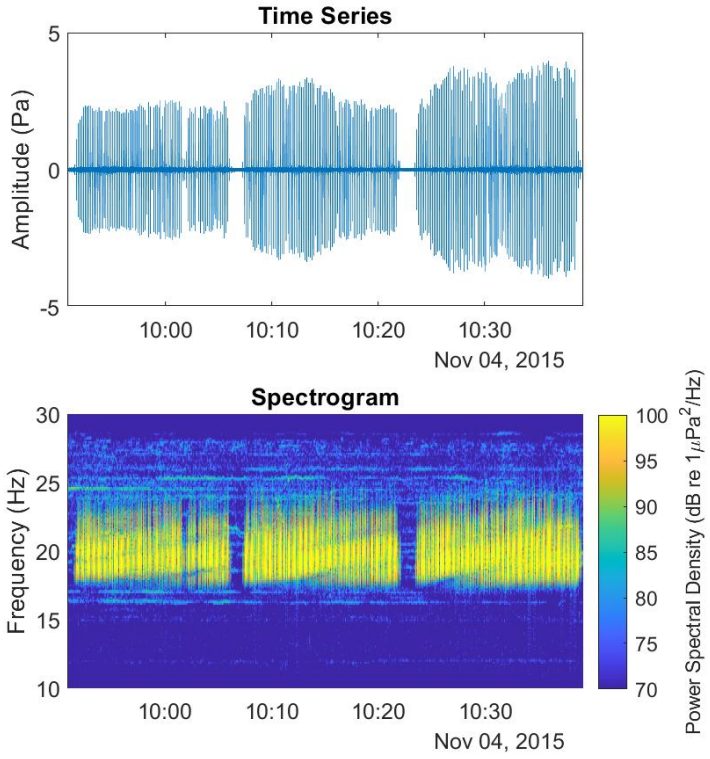

Figure 4.2. Time series (top) and spectrogram (bottom) of a segment of the fin whale bout recorded on a single hydrophone in Array 2 (hydrophone at 26 m depth) showing three separate songs. Data has been bandpass filtered to improve SNR of the 20-Hz pulses. Time axis is UTC.

Sequential pulses within a bout are relatively constant in level, but the pulses immediately following or preceding a quiet period have been found to be of lower level in recordings made in both the Atlantic (Watkins et al., 1987) and North Pacific (Helble et al., 2020). This phenomenon was also observed in the recorded signal bout. No explanation has been provided for these lower levels, but it has been theorized that they could be due to lower source levels from the fin whale or due to higher acoustic transmission loss when the whale is closer to the surface (Helble et al., 2020), assuming the whale is surfacing during the rest periods.

4.4.1 Bout Properties

The median interpulse interval measured between the peaks of successive pulses throughout the bout was 9.6 seconds. This measurement is consistent with previously recorded intervals presented in Morano et al. (2012) and Watkins et al. (1987) for fin whales in the western North Atlantic during this time of year. Throughout the entire recorded bout there were periodic rests in vocalizations that occurred at regular intervals where the 20-Hz pulses would occur for 14 minutes (median value) and then there would be a quiet period of 112 seconds (median value) before the pulses began again. Watkins et al. (1987) reported periodic rests within a bout averaging 115 seconds roughly every 15 minutes, which is consistent with the pattern seen with the bout recorded off Rhode Island. These rest periods have been correlated to a whale surfacing (Cummings et al., 1986), but sometimes a whale will stop vocalizing for a short period of time without surfacing (Watkins et al., 1987).

4.4.2 Received Levels

The received sound pressure level recorded during the fin whale bout was generally higher on Array 2 as compared to Array 1. The maximum received level of the mode one arrival on Array 1 was 129 dB re 1μPa (peak) and was 143 dB re 1μPa (peak) on Array 2. The higher received levels recorded on Array 2 suggest that the whale traveled closer to this array than Array 1 (Figure 4.3 (top)).

4.4.3 Range Difference

The difference in arrival time of individual 20-Hz pulses on a single sensor in each array was measured. This difference in arrival time was used to calculate the range difference of the whale between the arrays (Figure 4.3 (bottom)). The maximum difference in range is 7.5 km, which is the spacing between the two

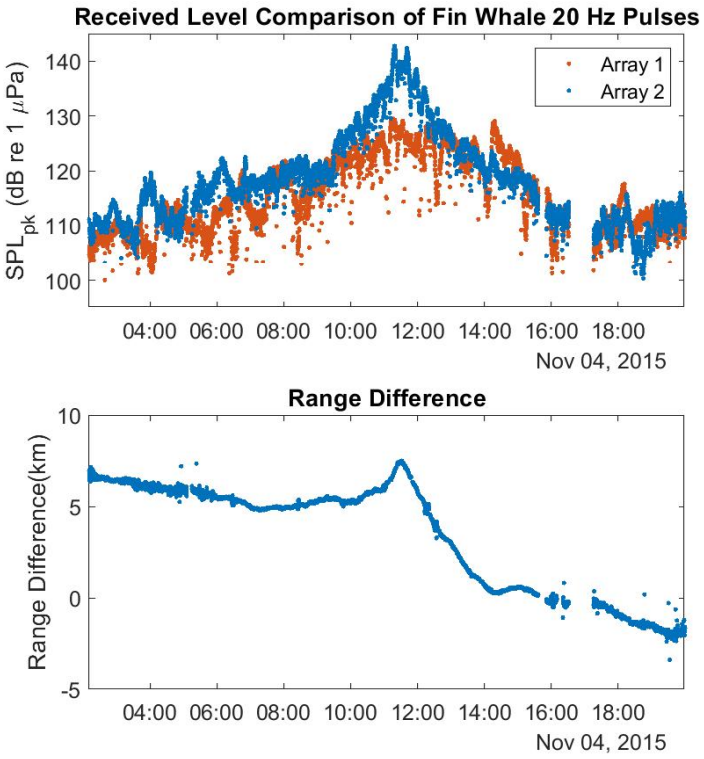

Figure 4.3. Comparison of the peak sound pressure levels (dB re 1μPa) of the 20-Hz pulse measured on both arrays throughout the recorded bout (top). Difference in the path length of the fin whale signals received on a single sensor in both arrays. A positive distance means the signal was received on Array 2 before Array 1 and a negative distance means the signal was received on Array 1 before Array 2 (bottom). The hydrophone used to generate these data is at a depth of 25 m on Array 1 and 26 m on Array 2. Time axis is UTC.

arrays. This maximum difference in range would be expected when the whale's position was directly in line with the two arrays, which would imply the signal arrived on Array 2 first and then traveled 7.5 km before reaching Array 1.

The received levels recorded on Array 2 were higher than those recorded on Array 1 up through approximately 13:00, before the received levels became similar on both arrays (Figure 4.3 (top)). This suggests that the whale was closer to Array 2 up until this time and then the whale traversed a track that was a similar distance from both arrays. This is confirmed by the variation in the range difference. As

the whale approaches the arrays, it is farther from Array 1 than it is from Array 2. The range difference between arrivals is maximum at 11:30, which coincides with the time of the maximum received sound levels measured on Array 2. This is the time of the closest point of approach of the whale to the arrays. As the whale moves away from the arrays, it follows a path bringing it closer to Array 1. After 16:00 it is traveling a path that is closer to Array 1 than Array 2.

4.5 Verification of Detections

A moored buoy system designed to detect, classify, and report the sounds of large whales in near real time that was part of a separate study (Baumgartner and Lin, 2019) was deployed near Martha's Vineyard, Massachusetts, USA during the same time that the arrays in this study were deployed. The buoy was 45 km east of Array 1 and 42 km east of Array 2 (Figure 4.1) in a water depth of 34 m and was equipped with a digital acoustic monitoring (DMON) instrument that was running a low frequency detection and classification system (LFDCS). The DMON/LFDCS detects and classifies tonal sounds of baleen whales in near real time and sends the detection data shore-side to be reviewed. The number of species specific detections in a 15-minute period within the acoustic detection range of the buoy were made available to the public after they had been verified.

The DMON/LFDCS automatically detects and classifies fin whales based on the 20-Hz pulse. Fin whales detected by the DMON/LFDCS had the lowest missed detection rate compared to other species and had a near real-time false detection rate of nearly 0 percent. The DMON/LFCDS system was not used for localization, but the fin-whale specific acoustic detection range of the system was estimated at 30-40 km (Baumgartner and Lin, 2019). This estimate was based on acoustic detections and visual sightings at 40 km spatial scales and 24-72 hr temporal scales. It is possible that the detection range is less or more than this spatial scale since

the acoustic and visual detections were not simultaneous, although this detection range was consistent with the 30 km detection range determined by Cholewiak et al. (2018) in a similar shallow environment of Massachusetts Bay.

The detection record of fin whales on November 4, 2015 showed that the DMON/LFDCS detected the largest number of fin whale 20-Hz pulses about 6 hours and 45 minutes before the highest sound levels were measured on the arrays (Figure 4.4). It is assumed that the pulses recorded on the arrays were made by a single fin whale and that the DMON detections are of that same whale. Examples of DMON recorded data show a single fin whale 20-Hz pulse that repeats at regular intervals of approximately every 10 seconds (pitch track (PT) data for 11/03/15 23:19:32 EST available on http://dcs.whoi.edu/nomans0315/nomans0315.shtml), which is similar to what was recorded on the arrays. From the time series of DMON/LFDCS detections it was inferred that the fin whale traveled through the detection range of the system toward the array locations and was beyond the detection range of the DMON at the time of the highest measured sound levels on the arrays. Since the arrays were able to detect the fin whale calls during the earlier times, it is assumed that the detection range of the arrays is farther than the 40 km DMON detection range.

4.6 Mode Dispersion and Source Localization

The normal mode approach is typically used to describe low frequency sound propagation in shallow water environments. A mode is described as a standing wave between the boundaries of an acoustic waveguide that propagates horizontally with a frequency dependent speed (Jensen et al., 2011). The group velocity of a mode is the velocity at which energy in the mode is transported. A signal measured on a receiver will be the summation of all of the modes, however, individual modes traveling at different group velocities will arrive at different times (Urick, 1983).

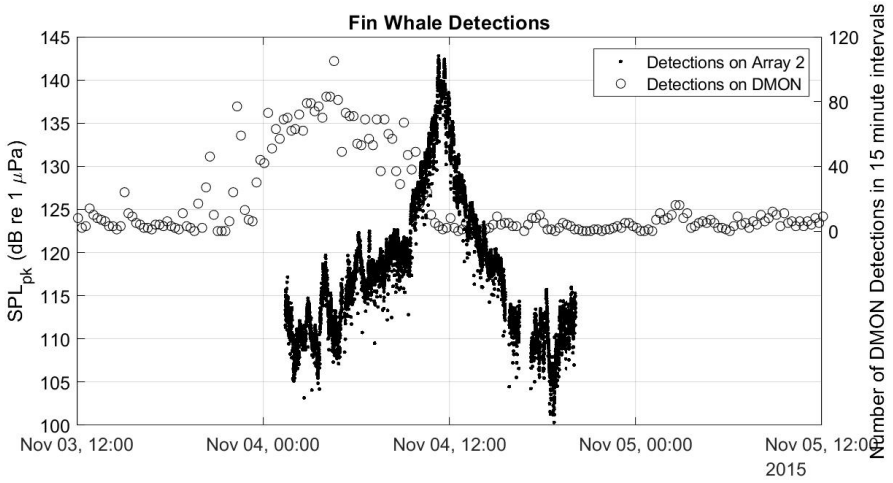

Figure 4.4. Comparison of the peak sound pressure levels (dB re 1μPa (peak)) recorded on Array 2 and the number of fin whale detections on the DMON buoy on November 4, 2015. Time axis is UTC.

4.6.1 Modal Arrivals

Two distinct modal arrivals of individual 20-Hz pulses were observed in the data recorded by the arrays (Figure 4.5). The mode one arrival of the 20-Hz pulse was detected by cross correlating the time series with a representative 20-Hz pulse. The representative pulse used was selected from the data as a pulse that had a high signal to noise ratio and only one modal arrival. Correlations above a threshold were classified as detections and saved for further analysis. All detections were manually verified and false detections were disregarded.

The mode two arrival arrived before the mode one arrival (Figure 4.5). The amplitude of mode one was larger than the amplitude of mode two (Figure 4.6). The mode two arrivals were detected by finding peaks in the envelope of the time series signal above a threshold that arrived before the largest amplitude detection. All detections were manually verified and false detections were disregarded. The lower amplitude modal arrivals that had a peak-signal to rms-noise ratio above 15 dB were included in further analysis. Multiple modes were not detected prior

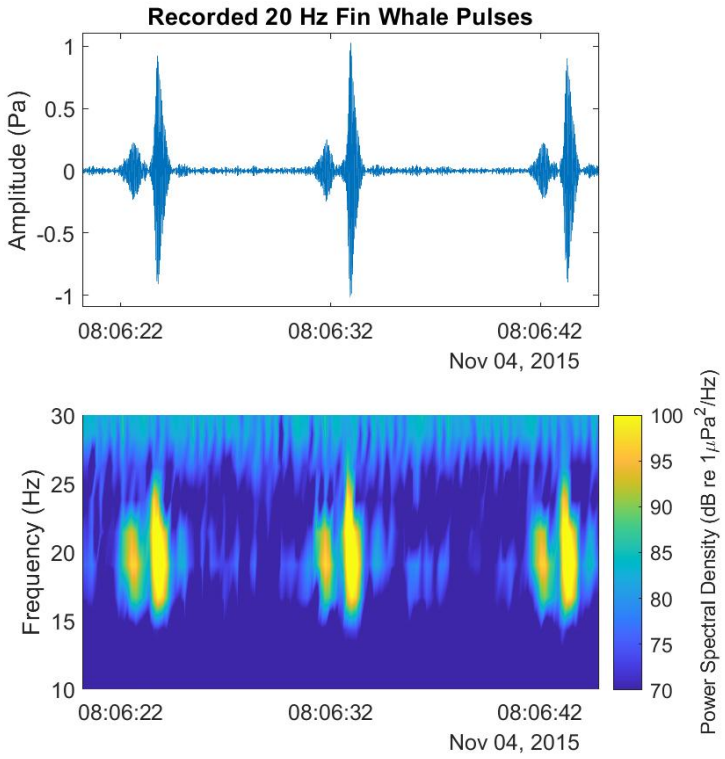

Figure 4.5. Time series (top) and spectrogram (bottom) showing three fin whale 20-Hz pulses recorded on a single hydrophone in Array 1. Two distinct and time separated arrivals are clearly seen in both the time series and spectrogram representation. The interpulse interval between the larger amplitude arrivals (mode one) is approximately 10 seconds. The receiver was at 25 meters depth. Time axis is UTC.

to 07:00 and later than 15:30 in the dataset because the SNR of the higher order modes was not greater then the ambient noise levels.

4.6.2 Time Delay between Modal Arrivals

The time delay between the mode two and mode one arrivals within an individual 20-Hz pulse on a single sensor was calculated. The time delay data was smoothed by taking the average time delay in each song. The median song duration was 14 minutes long, so the average time delay was taken every 14 minutes.

The time delay between the arrivals in the mode pairs from Figure 4.6 was

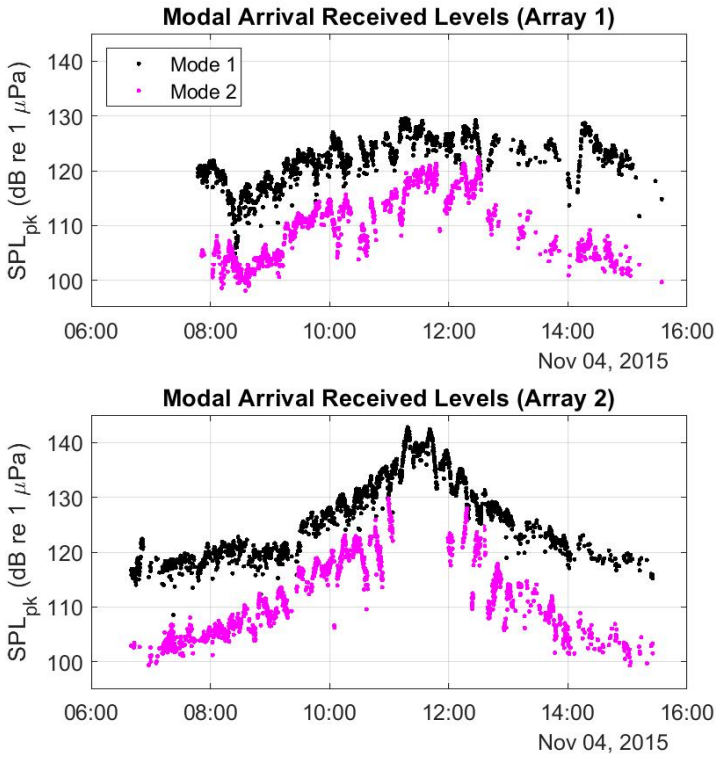

Figure 4.6. Peak sound pressure levels (dB re 1μPa (peak)) of the individual modal arrivals on a single sensor in each array. The sensor was at a depth of 25 m in Array 1 and 26 m in Array 2. Time axis is UTC.

calculated. The time difference between the modal arrivals on a single hydrophone varied throughout the recording (Figure 4.7) and was a function of the range of the whale from the sensor. The time difference between arrivals was greater at earlier times and decreased as the whale approached the array. Only one arrival was identifiable in the data from Array 2 when the whale was closest, although two arrivals were seen in the data from Array 1 during this same time.

4.6.3 Range Estimate

The range of the whale from each array was calculated using Equation 4.1, where R is the range of the whale in meters, v is the group speed of the indicated modal arrival, and Δt is the difference in arrival time between the two modes as

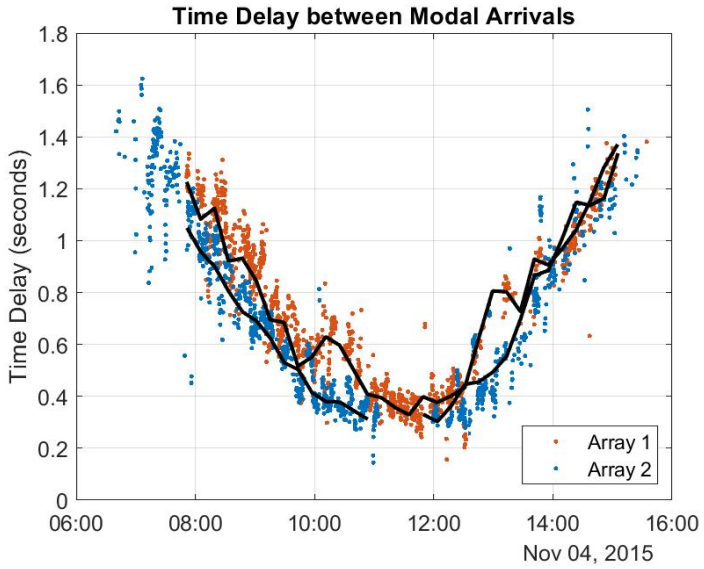

Figure 4.7. Time delay (in seconds) between the mode two and mode one arrivals in the records of both arrays when two modes could be resolved in the received time series. The average time delay in 14-minute time intervals (representing indidivudal songs) was calculated to smooth the data. Black lines are the average modal time delays for the individual songs in the bout. These average time delays were used to determine the range of the whale from the arrays. Time axis is UTC.

measured in the received signal of a single sensor. The modal group speeds are unknown, but the measured range difference (Figure 4.3 (bottom)) was used to limit the range estimate. The measured modal time delays from Figure 4.7 and estimates of the modal group speeds were used to calculate the distance of the whale from each array. The range of the whale from both arrays was estimated assuming group speeds between 1400 and 1800 m/s. The root-mean-square error of the difference in the range estimate from Array 2 and Array 1 was determined. The combination of modal group speeds that resulted in the smallest root-mean-square error were considered the optimal group speeds.

$$R = \frac{v_2 v_1 \Delta t}{v_2 - v_1} \tag{4.1}$$

The range of the whale from both arrays (Figure 4.8) was calculated using

Equation 4.1 with these optimal modal group speeds(v_1, v_2) and the measured modal time delays (Δt). Since two distinct modal arrivals were not distinguishable on Array 2 during the closest point of approach, the range of the whale from Array 2 during this time was not able to be resolved using the modal time delay. However the difference in range between the two arrays was used to determine the whale range during this time frame. The estimated range of the whale from Array 1 was adjusted by the range difference to yield an estimate of the whale range from Array 2 (Figure 4.8 (black line)). The range estimated using both methods was similar during the whale approach and departure, but the estimate using the range difference was able to resolve the closest point of approach of the whale from Array 2.

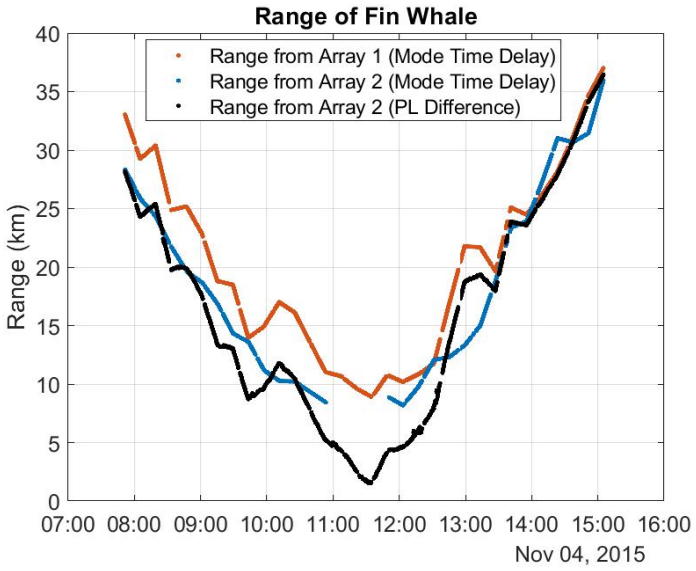

Figure 4.8. Estimated range of the whale from each array that was calculated assuming a group speed of 1563 m/s for mode one and a group speed of 1659 m/s for mode 2 (blue and orange lines). The whale's range from Array 2 when it was closest could not be resolved using the time difference between modes, so the range was estimated using the difference in range (black line). The two methods of calculating the whale range from Array 2 compare well during the approach and departure of the whale. Time axis is UTC.

4.6.4 Estimate of Whale Track

The estimate of the whale's range from both arrays was used to determine the whale's track. At each time step, a circle centered on each array with a radius equal to the range of the whale from that array was drawn. The intersection of the two range circles was a potential location of the whale. There were two intersection points for each time step, which yielded two potential whale tracks. Since the fin pulses were detected on the DMON buoy before the arrays, the whale was assumed to be traveling from the northeast, so tracks that showed the whale traveling from the southwest were disregarded. Also large number of fin whale calls were not detected on the DMON after 12:00 (Figure 4.4) and it is unlikely that this whale turned around to travel back towards the DMON location at any point during the track. This is supported by observations of fin whale singers that been tracked swimming with fairly consistent directions of travel (Clark et al., 2019). Therefore, the localization that produced a track with the fin whale traveling from northeast to southwest was determined to be the most plausible track (Figure 4.9).

4.6.5 Speed and Track of Whale

The whale was tracked for a total distance of 73.5 km for a duration of 7.2 hours. The average swim speed of the whale along this track was 10.2 km/hr. This is consistent with fin whale speeds and tracks that have been previously reported in literature. Clark et al. (2019) tracked fin whales as they sang for 15.8 hours (mean) and traveled 86.2 km (mean) at speeds of 6.7 km/hr (mean). Fin whales in the North Pacific were tracked while they swam distances of 18 km (mean) over 6.9 hours (mean) at speeds of 3 km/hr (mean) (Soule and Wilcock, 2013). Kuna and Nábělek (2021) also tracked whales in the North Pacific as they covered distances between 16-38 km at speeds between 4.1 and 10.3 km/hr.

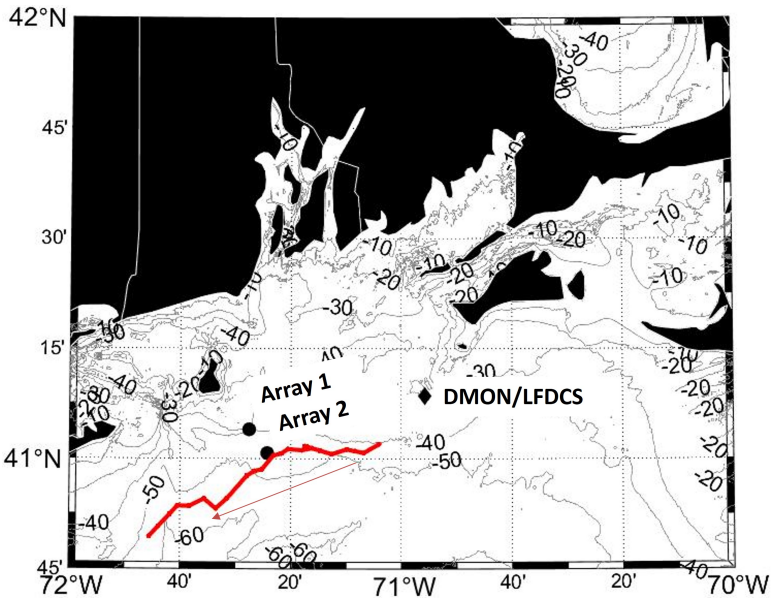

Figure 4.9. Most plausible path that the fin whale traveled on November 4, 2015 between 07:00 and 15:30 past the locations of the deployed arrays. Arrow indicates the direction of travel from northeast to southwest.

4.7 Conclusion

A fin whale was recorded vocalizing for over eighteen hours on two vertical line arrays that were deployed off the coast of Block Island, Rhode Island, USA. The 20-Hz pulses were emitted with a regular interpulse interval as the whale traveled a northeast to southwest track past the array locations. The signal received on the vertical line arrays arrived as two distinct modes, with mode two arriving before mode one due to the higher group velocity of the second mode. The 20-Hz pulses observed in this dataset were a single call that arrived as two arrivals due to modal dispersion and support the hypothesis that the fin whale doublet calls could be mulitpath arrivals and not produced as a doublet by the whale. The time delay between the modal arrivals on a single hydrophone and the time difference in arrival between the mode one arrival on two spatially separated hydrophones were used to determine the most likely range and track of the whale from the sensors. Fin whale detections on a separate system were used to inform the estimated whale

track.

Acknowledgments: The data used for this research was collected as part of the U.S. Department of the Interior, Bureau of Ocean Energy Management (BOEM), Environmental Studies Program, Washington, DC under Contract Number M15PC00002, Task Order M16PD00025. Collaborators in this project include Randy Gallien and Anwar Khan (HDR, Inc.).

Bibliography

Baumgartner, M. F. and Lin, Y.-T. (2019). Evaluating the Accuracy and Detection Range of a Moored Whale Detection Buoy near the Massachusetts Wind Energy Area. Technical report, Woods Hole (MA): Massachusetts Clean Energy Center and U.S. Department of the Interior, Bureau of Ocean Energy Management.OCS Study BOEM 2019-061.

Castellote, M., Clark, C. W., and Lammers, M. O. (2012). Fin whale (Balaenoptera physalus) population identity in the western Mediterranean Sea. *Marine Mammal Science*, 38:325–344.

Cholewiak, D., Clark, C. W., Ponirakis, D., Frankel, A. S., Hatch, L. T., Risch, D., Stanistreet, J. E., Thompson, M., Vu, E., and Van Parijs, S. M. (2018). Communicating amidst the noise: modeling the aggregate influence of ambient and vessel noise on baleen whale communication space in a national marine sanctuary. *Endangered Species Research*, 36:59–75.

Clark, C. W., Gagnon, G. J., and Frankel, A. S. (2019). Fin whale singing decreases with increased swimming speed. *Royal Society Open Science*, 6.

Croll, D. A., Clark, C. W., Acevedo, A., Tershy, B., Flores, S., Gedamke, J., and Urban, J. (2002). Only male fin whales sing loud songs. *Nature*, 417:809.

Cummings, W. C., Thompson, P. O., and Ha, S. J. (1986). Sounds from Bryde, Balaenoptera edeni, and finback, B. physalus, whales in the Gulf of California. *Fishery Bulletin*, 84(2):359–370.

Frisk, G. V. (1994). *Ocean and Seabed Acoustics*. Prentice-Hall, Inc, Englewood Cliffs, New Jersey.

Rebull, O. G., Cusí, J. D., Ruiz Fernández, M., and Muset, J. G. (2006). Tracking fin whale calls offshore the Galicia Margin, North East Atlantic Ocean. *The Journal of the Acoustical Society of America*, 120(4):2077–2085.

HDR (2018). Benthic Monitoring During Wind Turbine Installation and Operation at the Block Island Wind Farm , Rhode Island. Technical report, Final Report to the U.S. Department of the Interior, Bureau of Ocean Energy Management, Office of Renewable Energy Programs.

Helble, T. A., Guazzo, R. A., Alongi, G. C., Martin, C. R., Martin, S. W., and Henderson, E. E. (2020). Fin Whale Song Patterns Shift Over Time in the Central North Pacific. *Frontiers in Marine Science*, 7.

Jensen, F. B., Kuperman, W. A., Porter, M. B., and Schmidt, H. (2011). *Computational Ocean Acoustics*. Springer Science, New York, NY, second edition.

Kuna, V. M. and Nábělek, J. L. (2021). Seismic crustal imaging using fin whale songs. *Science*, 371:731–735.

Lin, Y.-T., Newhall, A. E., and Lynch, J. F. (2012). Low-frequency broadband sound source localization using an adaptive normal mode back-propagation approach in a shallow-water ocean. *The Journal of the Acoustical Society of America*, 131(2):1798–1813.

Lin, Y.-T., Newhall, A. E., Miller, J. H., Potty, G. R., and Vigness-Raposa, K. J. (2019). A three-dimensional underwater sound propagation model for offshore wind farm noise prediction. *The Journal of the Acoustical Society of America*, 145(5):EL335–EL340.

Mikhalevsky, P. N (2001). *Arctic Acoustics*. Encyclopedia of Ocean Sciences, J.H. Steele, ed., vol. 1, pp 53-61, Elsevier Ltd.

Miksis-Olds, J. L., Harris, D. V., and Heaney, K. D. (2019). Comparison of estimated 20-Hz pulse fin whale source levels from the tropical Pacific and Eastern North Atlantic Oceans to other recorded populations. *Journal of the Acoustical Society of America*, 146(4):2373–2384.

Morano, J. L., Salisbury, D. P., Rice, A. N., Conklin, K. L., Falk, K. L., and Clark, C. W. (2012). Seasonal and geographical patterns of fin whale song in the western North Atlantic Ocean. *The Journal of the Acoustical Society of America*, 132(2):1207–1212.

Needell, S. W., O'Hara, C. J., and Knebel, H. J. (1983). Maps showing geology and shallow structure of western Rhode Island Sound: U.S. Geological Survey Miscellaneous Field Studies Map MF-1537. Technical report, U.S. Geological Survey.

Nieukirk, S. L., Mellinger, D. K., Moore, S. E., Klinck, K., Dziak, R. P., and Goslin, J. (2012). Sounds from airguns and fin whales recorded in the mid-Atlantic Ocean , 1999-2009. *The Journal of the Acoustical Society of America*, 131(2):1102–1112.

Porter, M. B. (1991). The KRAKEN Normal Mode Program. Technical report, SACLANT Underwater Research Centre, La Spezia, Italy.

Premus, V. and Spiesberger, J. L. (1997). Can acoustic multipath explain finback (B. physalus) 20-Hz doublets in shallow water? *The Journal of the Acoustical Society of America*, 101:1127–1138.

Sheldon, D. P. H. (2012). *Stratigraphy of a Proposed Wind Farm Site Southeast of Block Island: Utilization of Borehole Samples, Downhole Logging, and Seismic Profiles*. PhD thesis, University of Rhode Island.

Širović, A., Hildebrand, J. A., and Wiggins, S. M. (2007). Blue and fin whale call source levels and propagation range in the Southern Ocean Blue and fin whale call source levels and propagation range in the Southern Ocean. *The Journal of the Acoustical Society of America*, 122(2):1208–1215.

Soule, D. C. and Wilcock, W. S. D. (2013). Fin whale tracks recorded by a seismic network on the Juan de Fuca Ridge, Northeast Pacific Ocean. *The Journal of the Acoustical Society of America*, 133(3):1751–1761.

Stafford, K. M., Mellinger, D. K., Moore, S. E., and Fox, C. G. (2007). Seasonal variability and detection range modeling of baleen whale calls in the Gulf of Alaska, 1999â€“2002. *The Journal of the Acoustical Society of America*, 122(6):3378–3390.

Thompson, P. O., Findley, L. T., and Vidal, O. (1992). 20-Hz pulses and other vocalizations of fin whales, Balaenopteraphysalus, in the Gulf of California, Mexico. *The Journal of the Acoustical Society of America*, 92(6):3051–3057.

Urick, R. J. (1983). *Principles of Underwater Sound*. Peninsula Publishing, Los Altos, CA, 3rd edition.

Watkins, W. A. (1981). Activities and Underwater Sounds of Fin Whales. *Sci. Rep. Whales Res. Inst*, 33:83–117.

Watkins, W. A., Tyack, P., Moore, K. E., and Bird, J. E. (1987). The 20-Hz signals of finback whales (Balaenoptera physalus). *The Journal of the Acoustical Society of America*, 82(6):1901–1912.

Weirathmueller, M. J., Stafford, K. M., Wilcock, W. S. D., Hilmo, R. S., Dziak, R. P., and Trehu, A. M. (2017). Spatial and temporal trends in fin whale

vocalizations recorded in the NE Pacific Ocean between 2003-2013. *PLOS One*, 12(10).

Wiggins, S. M., McDonald, M. A., Munger, L. M., Moore, S. E., and Hildebrand, J. A. (2004). Wavegu ide Propagation allows for Range Estimates for North Pacific Right Whales in the Bering Sea. *Canadian Acoustics*, 32(2):146–154.